Resource

EMBO reports

# Somatosensory neurons express specific sets of lincRNAs, and lincRNA CLAP promotes itch sensation in mice

Bin Wang[1,2,*,†], Bowen Jiang[1,†], Guo-Wei Li[3,†], Fei Dong[4], Zheng Luo[3], Bing Cai[2], Manyi Wei[1], Jiansong Huang[1], Kaikai Wang[2,5], Xin Feng[1], Fang Tong[6], Sashuang Wang[2,7], Qiong Wang[1], Qingjian Han[6], Changlin Li[2,8], Xu Zhang[2,4,5,8], Li Yang[9,**] & Lan Bao[1,5,***]

## Abstract

**Somatosensory neurons are highly heterogeneous with distinct types of neural cells responding to specific stimuli. However, the distribution and roles of cell-type-specific long intergenic noncoding RNAs (lincRNAs) in somatosensory neurons remain largely unexplored. Here, by utilizing droplet-based single-cell RNA-seq (scRNA-seq) and full-length Smart-seq2, we show that lincRNAs, but not coding mRNAs, are enriched in specific types of mouse somatosensory neurons. Profiling of lincRNAs from single neurons located in dorsal root ganglia (DRG) identifies 200 lincRNAs localized in specific types or subtypes of somatosensory neurons. Among them, the conserved cell-type-specific lincRNA *CLAP* associates with pruritus and is abundantly expressed in somatostatin (SST)-positive neurons. *CLAP* knockdown reduces histamine-induced $Ca^{2+}$ influx in cultured SST-positive neurons and *in vivo* reduces histamine-induced scratching in mice. *In vivo* knockdown of *CLAP* also decreases the expression of neuron-type-specific and itch-related genes in somatosensory neurons, and this partially depends on the RNA binding protein MSI2. Our data reveal a cell-type-specific landscape of lincRNAs and a function for *CLAP* in somatosensory neurons in sensory transmission.**

**Keywords** cell-type-specific lincRNA; itch sensation; scRNA-seq; somatosensory neuron

**Subject Categories** Neuroscience; RNA Biology

**DOI** 10.15252/embr.202154313 | Received 11 November 2021 | Revised 16 November 2022 | Accepted 22 November 2022 | Published online 16 December 2022

**EMBO Reports (2023) 24: e54313**

## Introduction

Dorsal root ganglion (DRG) contains the cell body of somatosensory neurons that convey sensory information including thermal, mechanical, and chemical stimuli from the peripheral afferents to the central nervous system for brain perception (Basbaum *et al*, 2009). Decades of researches reveal that DRG neurons exhibit highly heterogeneity according to their size and gene expression. Recently, single-cell RNA sequencing (scRNA-seq) classifies DRG neurons into 10 types and 14 subtypes and reveals cell-type-specific expression of modulator mRNAs in sensory transmission especially for mechanical transduction and itch (Usoskin *et al*, 2015; Li *et al*, 2016, 2018; Stantcheva *et al*, 2016). Furthermore, combination of deep sequencing for genetically labeled subtype of DRG neurons with electrophysiological analysis identifies that ion channels mediate subtype-specific stimulus modalities (Zheng *et al*, 2019), suggesting a unique molecular signaling in DRG neurons. With rapid advance of RNA-seq technologies, a large number of noncoding RNAs, including long noncoding RNAs (lncRNAs), have been characterized and implicated in developmental and degenerative diseases (Briggs *et al*, 2015; Salta

1 State Key Laboratory of Cell Biology, Shanghai Institute of Biochemistry and Cell Biology, CAS Center for Excellence in Molecular Cell Science, University of Chinese Academy of Sciences, Chinese Academy of Sciences, Shanghai, China
2 Guangdong Institute of Intelligence Science and Technology, Zhuhai, China
3 CAS Key Laboratory of Computational Biology, Shanghai Institute of Nutrition and Health, University of Chinese Academy of Sciences, Chinese Academy of Sciences, Shanghai, China
4 Institute of Neuroscience and State Key Laboratory of Neuroscience, CAS Center for Excellence in Brain Science and Intelligence Technology, Shanghai, China
5 School of Life Science and Technology, ShanghaiTech University, Shanghai, China
6 State Key Laboratory of Medical Neurobiology, MOE Frontiers Center for Brain Science, Institutes of Brain Science, Fudan University, Shanghai, China
7 Department of Pain Medicine and Shenzhen Municipal Key Laboratory for Pain Medicine, Huazhong University of Science and Technology Union Shenzhen Hospital, Shenzhen, China
8 Research Unit of Pain, Chinese Academy of Medical Sciences, Shanghai Advanced Research Institute, Chinese Academy of Sciences, Shanghai, China
9 Center for Molecular Medicine, Children's Hospital, Fudan University and Shanghai Key Laboratory of Medical Epigenetics, International Laboratory of Medical Epigenetics and Metabolism, Ministry of Science and Technology, Institutes of Biomedical Sciences, Fudan University, Shanghai, China
*Corresponding author. Tel: +86 756 2898999; E-mail: wangbin@gdiist.cn
**Corresponding author. Tel: +86 21 54237325; E-mail: liyang_fudan@fudan.edu.cn
******Corresponding author. Tel: +86 21 54921369, Fax: +86 21 54921762; E-mail: baolan@sibcb.ac.cn
†These authors contributed equally to this work

& De Strooper, 2017). Application of scRNA-seq and precise cell-type classification in DRG neurons provide opportunities to study regulatory functions of cell-type-specific lncRNAs in these neurons.

A subclass of lncRNAs, long intergenic noncoding RNAs (lincRNAs) transcribed from intergenic regions, have been recently shown to play pivotal roles in different biological processes (Ransohoff *et al*, 2018; Carlevaro-Fita & Johnson, 2019; Yao *et al*, 2019). Bioinformatic analysis revealed that lincRNAs constitute more than half of lncRNA transcripts in human transcriptomes (Ransohoff *et al*, 2018). According to an early study, 78% of human lincRNAs exhibit tissue specificity compared with 19% of mRNAs especially in the brain (Cabili *et al*, 2011), implying possible fine-tuning of lincRNAs in a tissue- and cell-type-specific manner. Although previous studies showed that lncRNA Kcna2 antisense RNA and *Silc1* involved in neuropathic pain and nerve regeneration in DRG neurons (Zhao *et al*, 2013; Perry *et al*, 2018), the landscape and functions of cell-type-specific lincRNAs in DRG neurons remained largely unknown.

In the present study, combined our scRNA-seq datasets from droplet-based (also known as 10× Genomics) and full-length Smart-seq2, we firstly constructed a single-cell lincRNA landscape of DRG cells and identified 200 lincRNAs highly expressed in distinct types and subtypes of mouse DRG neurons. Furthermore, we characterized a previously unknown lincRNA *9130409J20Rik*, referred to as *CLAP* (Cell-type-specific LincRNA Associating with Pruritus), which is highly conserved and specifically expressed in somatostatin-positive neurons for histamine-mediated neuronal activation and pruritus. Our findings thus provide a rich resource of lincRNAs in sensory transmission and greatly expand the knowledge of cell-type-specific function of lincRNA in itch sensation.

## Results

### lincRNAs are profiled by 10× Genomics scRNA-seq in DRG neurons

We reused our recently published 10× Genomics scRNA-seq dataset (Wang *et al*, 2021), which was not applied for lincRNA profiling, to identify cell-type-specific lincRNAs in DRG neurons at single-cell resolution (Fig 1A). In total, 7,935 dissociated cells from DRGs were classified by unsupervised graph clustering and then characterized with canonical marked genes, which led to the classification of 9 major cell populations including DRG neurons and other non-neuronal cell types (Fig EV1A) as recently reported (Wang *et al*, 2021).

From 6,864 annotated lincRNAs (87% of total lncRNAs) in Ensemble and Refseq (Fig EV1B and C), an average number of 192 ± 54 lincRNAs was detected in single neuron along with 6,288 ± 1,121 mRNAs, which were more than those in other non-neuronal cells within the DRG (Fig 1B). To determine the abundance of lincRNAs in various cells of DRG, we analyzed the median expression level of mRNAs and lincRNAs per cell by combining results of single cell with bulk tissue *in silico* as previously reported (Liu *et al*, 2016). The results showed that the single-cell level of lincRNAs was greatly lower than that of mRNAs, especially for the neurons (mRNA: 6.92, lincRNA: 0.14; Fig 1C). Meanwhile, the ratio of mRNA to lincRNA levels in neurons was 49.50, much higher than that in non-neuronal cells (Fig 1C). Although lincRNAs were much lowly expressed than mRNAs (Fig 1C), they tended to be expressed in specific cell population, especially for neurons. For instance, the majority of highly expressed lincRNAs were specifically distributed in a small group of neurons (0.67%), whereas high level of mRNAs was expressed universally in DRG neurons (25.20%; Fig 1D). To further confirm lincRNA heterogeneity in single-cell resolution, we calculated the coefficient of variation (CV; Mantsoki *et al*, 2016) for either lincRNAs or mRNAs. Obviously, the CV of lincRNAs (14.21) was much higher than that of mRNAs (2.31) in single neuron (Fig 1E), indicating the heterogeneity of lincRNAs within neurons.

### lincRNAs display a highly neuron-type-specific expression pattern in DRG neurons

To identify cell-type-specific lincRNAs in different DRG neurons, we applied specificity measure (SPM) analysis (Xiao *et al*, 2010) to quantitatively estimate the gene specificity in given samples, based on the mean level of individual lincRNA in each type of cells. The SPM was ranged from 0, suggesting no cell-type specificity, to 1, indicating an absolute specificity in the designated cell type. As indicated in Fig 1F, the percentage of neuron-type-specific lincRNAs greatly increased with rising SPM value, whereas the percentage of mRNAs slightly elevated. About 48% highly cell-type-specific lincRNAs (SPM ≥ 0.8) were distributed in neurons, whereas only 28% highly cell-type-specific mRNAs (SPM ≥ 0.8) were localized in neurons (Fig 1F), suggesting a greater type-specificity of lincRNAs than mRNAs in DRG neurons. Of note, the majority of those neuron-specific lincRNAs displayed clustered distribution (Fig EV1D; Dataset EV1), implying a preferential localization of those lincRNAs in distinct subsets of DRG neurons. Therefore, these results suggest an enriched distribution of lincRNAs in DRG neurons.

Multiple types of neurons have been classified in DRG neurons (Li *et al*, 2016). Given the highly specific expression of lincRNAs in DRG neurons, we next tempted to profile lincRNAs in different types of DRG neurons by combining those 10× Genomics datasets with our previously published Smart-seq2 datasets (Li *et al*, 2016), which was not applied for lincRNA profiling. Altogether, 1,818 DRG neurons by 10× Genomics and 197 DRG neurons by Smart-seq2 were classified into 10 types and 16 subtypes, respectively (Figs 2A and B, and EV2A and B). Given the fact that significantly more single DRG neurons were profiled by 10× Genomics (1,818) than Smart-seq2 (197), detailed subtypes of DRG neurons could be obtained by 10× Genomics. For example, totally five subtypes of C1 DRG neurons including C1-1 ($Gal^+/Cldn9^+$), C1-2-1 ($Gal^+/Zcchc12^+/Sstr2^+$), C1-2-2 ($Gal^+/Zcchc12^+/Dcn^+$), C1-2-3 ($Gal^+/Zcchc12^+/Trpm8^+$), and C1-2-4 ($Gal^+/Zcchc12^+/Rxfp1^+$) were clustered by 10× Genomics, while only one subtype of C1 ($Gal^+$) DRG neurons by Smart-seq2. Differently, due to lack of cell-size information by 10× Genomics, C6 ($S100b^+/Mrgprd^+$) and C10 ($S100b^+/Gal^+$) subtypes of DRG neurons were failed to be classified by 10× Genomics (Wang *et al*, 2021). Nevertheless, most subtypes of DRG neurons correlated well between 10× Genomics and Smart-seq2 datasets (Fig EV2C), providing a basis to integrate two datasets for subsequent analysis. In general, 1,092 ± 162 lincRNAs were detected by Smart-seq2 (Fig 2C), greater than that (192 ± 54) from those neurons by 10× Genomics (Figs 1B and 2C). We then analyzed the SPM of mRNAs and lincRNAs in the neuron types detected by Smart-seq2 and 10× Genomics. Importantly, the expression of lincRNAs and mRNAs displayed distinct bimodal distribution patterns: lincRNAs were

 

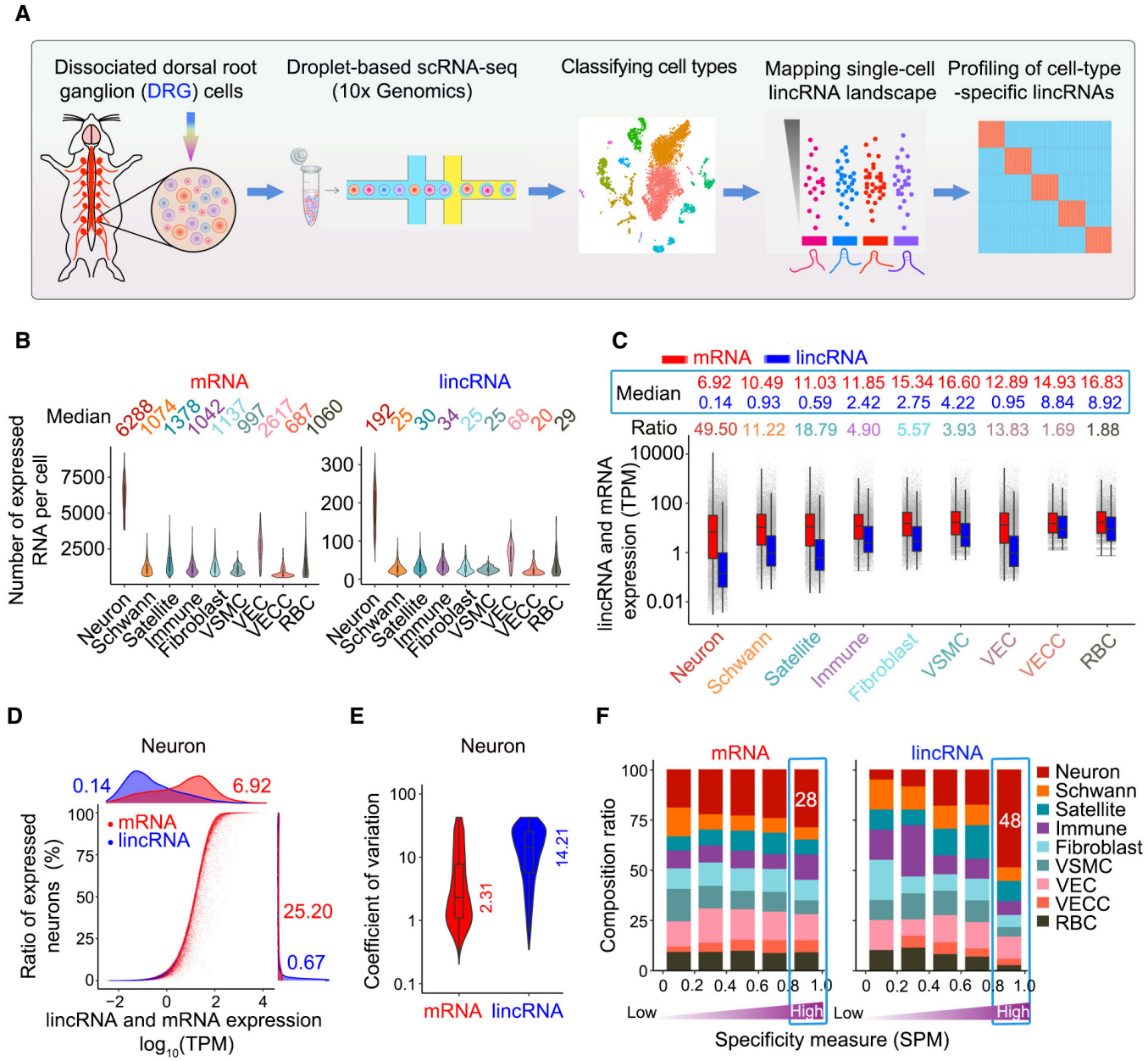


**Figure 1. Application of 10× Genomics scRNA-seq profiles for lincRNAs in the DRG.**

A Research flowchart showing the profiling of cell-type-specific lincRNAs by 10× Genomics in mouse DRGs.

B Violin plots showing the number of detected mRNAs and lincRNAs across distinct cell types by 10× Genomics. VSMC, vascular smooth muscle cell. VEC, vascular endothelial cell. VECC, vascular endothelial cell capillary. RBC, red blood cell.

C Dot plot showing the averagely single-cell level of mRNAs and lincRNAs in distinct cell types. Expression folds between mRNA and lincRNA were calculated by average level of mRNAs versus lincRNAs at single cell. TPM, transcript per million.

D Dot plot showed that majority of highly expressed lincRNAs were specifically expressed in a small population of neurons (0.67%), whereas mRNAs (25.2%) were expressed more broadly in neuron types by 10× Genomics.

E Dot plot showed that the coefficient of variation for lincRNAs was higher than mRNAs in the neuron type.

F Highly cell-type-specific lincRNAs (SPM ≥ 0.8) were more enriched in neuron types. Cell-type specificity of mRNAs and lincRNAs were calculated by specificity measure (SPM) in 10× Genomics.

Data information: Total 7,935 cells (analyzed in B, C, and F) and 1,818 neurons (analyzed in D and E) were collected from 2 replicates of 6 mice. In boxplot, central band, boxes, and whiskers represent median value, second/third quartiles and minimum/maximum value to second/third quartiles, respectively (B, C, and E).

distributed with high type specificity, whereas mRNAs were expressed more broadly across neuron types (Fig 2D). Furthermore, higher proportion of lincRNAs (41% by Smart-seq2 and 34% by 10× Genomics) exhibited neuron-type-specific pattern than those of mRNAs (23% by Smart-seq2 and 14% by 10× Genomics; Fig 2D). Consistently, the median SPM of lincRNAs in distinct neuron types

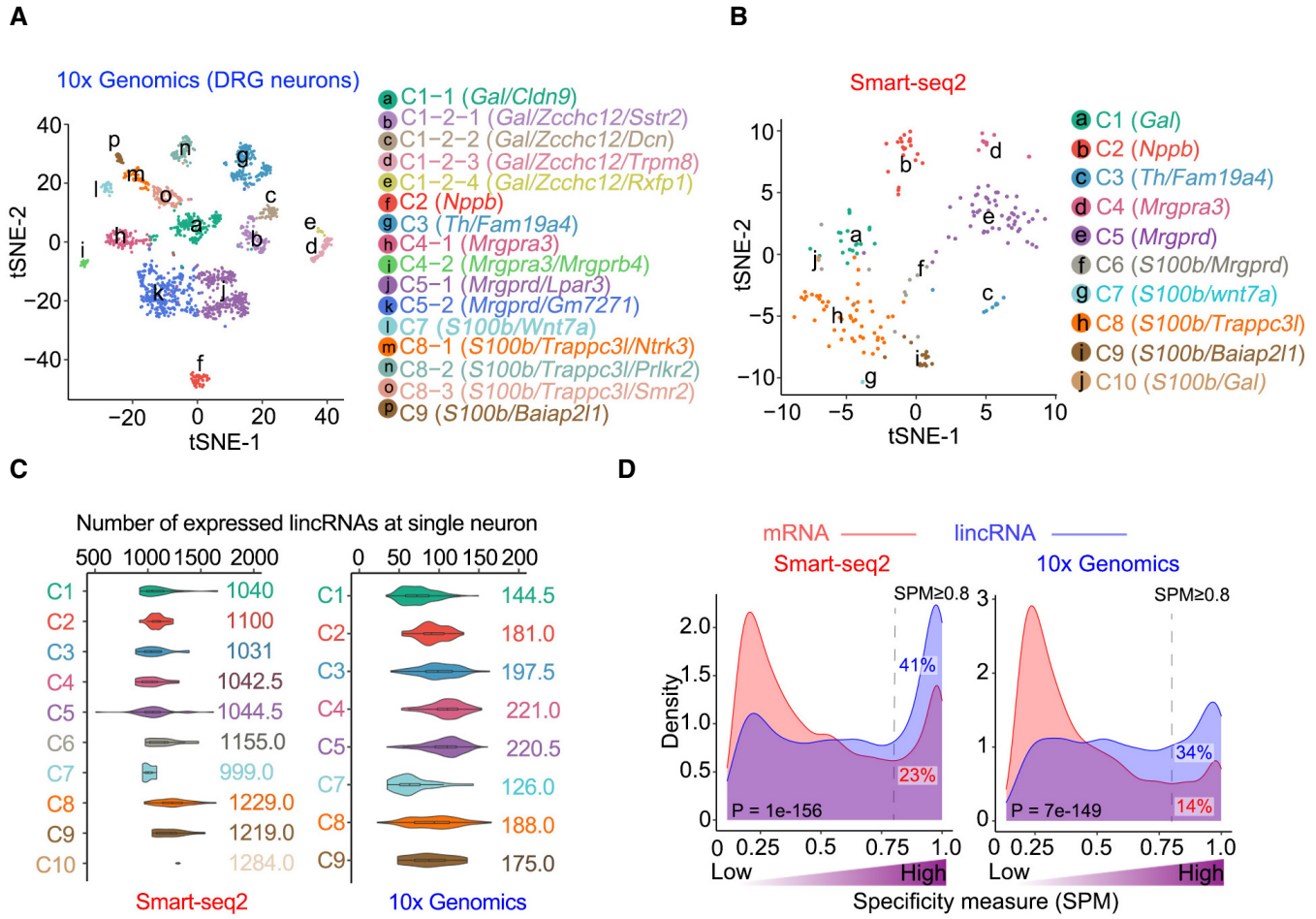


**Figure 2. lincRNAs are preferentially enriched in specific types of DRG neurons.**

A tSNE plot showing 16 cell types of 1,818 DRG neurons by 10× Genomics.

B tSNE plot showing 10 cell types of 197 DRG neurons by Smart-seq2.

C Boxplot showing the number of detected lincRNAs across distinct neuron types by two scRNA-seq methods.

D Density plot showed that lincRNAs exhibited higher neuron-type specificity than mRNAs in two scRNA-seq methods. Neuron-type specificity of mRNAs and lincRNAs was calculated by specificity measure (SPM).

Data information: Total 1,818 neurons from 10× Genomics (analyzed in A, C, and D) were collected from 2 replicates of 6 mice. And 197 neurons from Smart-seq2 (analyzed in B, C, and D) were collected from lumbar 5 DRG from five adult male mice as described in previous study. In boxplot, central band, boxes, and whiskers represent median value, second/third quartiles and minimum/maximum value to second/third quartiles, respectively (C).

**Figure 3. Landscape of neuron-type-specific lincRNAs in somatosensory neurons by Smart-seq2 and 10× Genomics.**

A Heatmap showing the neuron-type-specific lincRNAs consistently detected in two scRNA-seq methods. Rows represent specific cell types. Columns represent individual lincRNAs.

B Venn diagram showing the overlapping of highly neuron-type-specific lincRNAs ($SPM_{cluster} \geq 0.8$ and $TPM_{cluster} \geq 1$) between two scRNA-seq methods.

C Composition of 200 highly neuron-type-specific lincRNAs in distinct neuron types.

D Characterization of highly neuron-type-specific lincRNAs in two scRNA-seq methods, ranked by evaluation of robust rank aggregation (RRA) method.

E Representative images (Left) of smFISH in DRG section, tSNE plot of 10× Genomics (Middle), and quantitative result (Right) showed that *C530044C16Rik* was co-localized with *Gal-Cre*; Ai9 tdTomato neurons ($n = 7$), but not with *Sst-Cre* neurons ($n = 6$).

F Representative smFISH images (Left), tSNE plot of 10× Genomics (Middle), and quantitative result (Right) showed that *CLAP* was co-localized with *Sst-Cre*; Ai9 tdTomato neurons ($n = 6$), but not with *Gal-Cre* neurons ($n = 29$).

G Representative smFISH images (Left), tSNE plot of 10× Genomics (Middle), and quantitative result (Right) showed that *Gm11549* was co-localized with *Slc17a8-Cre*; Ai9 tdTomato neurons ($n = 5$), but not with *Mrgprd-Cre* neurons ($n = 6$).

H Representative smFISH images (Left), tSNE plot of 10× Genomics (Middle), and quantitative result (Right) showed that *2310002F09Rik* was co-localized with *Slc17a8-Cre*; Ai9 tdTomato neurons ($n = 6$), but not with *Slc17a8-Cre* neurons ($n = 6$).

I–K Representative images (Right) of double smFISH showed that *2310002F09Rik* was rarely co-localized with *C530044C16Rik* (I), *CLAP* (J) and *Gm11549* (K). Scale bar, 10 μm.

Data information: (E, F, G, H) The results are presented as mean ± SEM. *n* indicates the number of tissue sections at least from 3 mice.

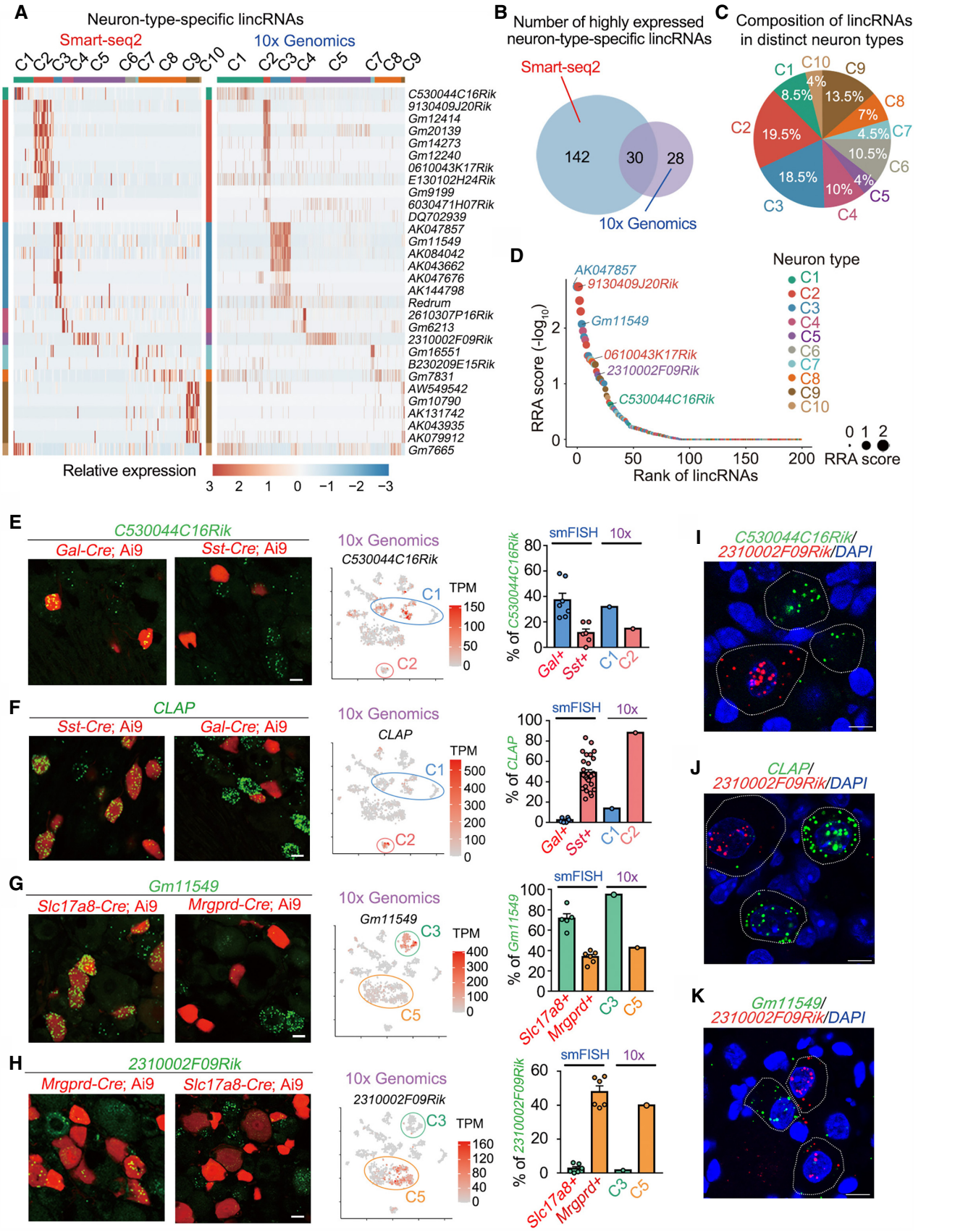
A
Neuron-type-specific lincRNAs
Smart-seq2
10x Genomics
C1 C2 C3 C4 C5 C6 C7 C8 C9 C10 C1 C2 C3 C4 C5 C7 C8 C9
C530044C16Rik
9130409J20Rik
Gm12414
Gm20139
Gm14273
Gm12240
0610043K17Rik
E130102H24Rik
Gm9199
6030471H07Rik
DQ702939
AK047857
Gm11549
AK084042
AK043662
AK047676
AK144798
Redrum
2610307P16Rik
Gm6213
2310002F09Rik
Gm16551
B230209E15Rik
Gm7831
AW549542
Gm10790
AK131742
AK043935
AK079912
Gm7665
Relative expression
3 2 1 0 −1 −2 −3
B
Number of highly expressed neuron-type-specific lincRNAs
Smart-seq2
142
30
28
10x Genomics
C
Composition of lincRNAs in distinct neuron types
C1 4%
C10 8.5%
C9 13.5%
C8 7%
C2 19.5%
C7 4.5%
C6 10.5%
C3 18.5%
C5 4%
C4 10%
D
AK047857
9130409J20Rik
Gm11549
0610043K17Rik
2310002F09Rik
C530044C16Rik
RRA score (-log10)
Rank of lincRNAs
Neuron type
C1 C2 C3 C4 C5 C6 C7 C8 C9 C10
0 1 2
RRA score
E
C530044C16Rik
Gal-Cre; Ai9
Sst-Cre; Ai9
10x Genomics
C530044C16Rik
TPM
150 100 50 0
smFISH 10x
% of C530044C16Rik
Gal+ Sst+ C1 C2
F
CLAP
Sst-Cre; Ai9
Gal-Cre; Ai9
10x Genomics
CLAP
TPM
500 400 300 200 100 0
smFISH 10x
% of CLAP
Sst+ Gal+ C1 C2
G
Gm11549
Slc17a8-Cre; Ai9
Mrgprd-Cre; Ai9
10x Genomics
Gm11549
TPM
400 300 200 100 0
smFISH 10x
% of Gm11549
Slc17a8+ Mrgprd+ C3 C5
H
2310002F09Rik
Mrgprd-Cre; Ai9
Slc17a8-Cre; Ai9
10x Genomics
2310002F09Rik
TPM
160 120 80 40 0
smFISH 10x
% of 2310002F09Rik
Slc17a8+ Mrgprd+ C3 C5
I
C530044C16Rik/
2310002F09Rik/DAPI
J
CLAP/
2310002F09Rik/DAPI
K
Gm11549/
2310002F09Rik/DAPI

**Figure 3.**

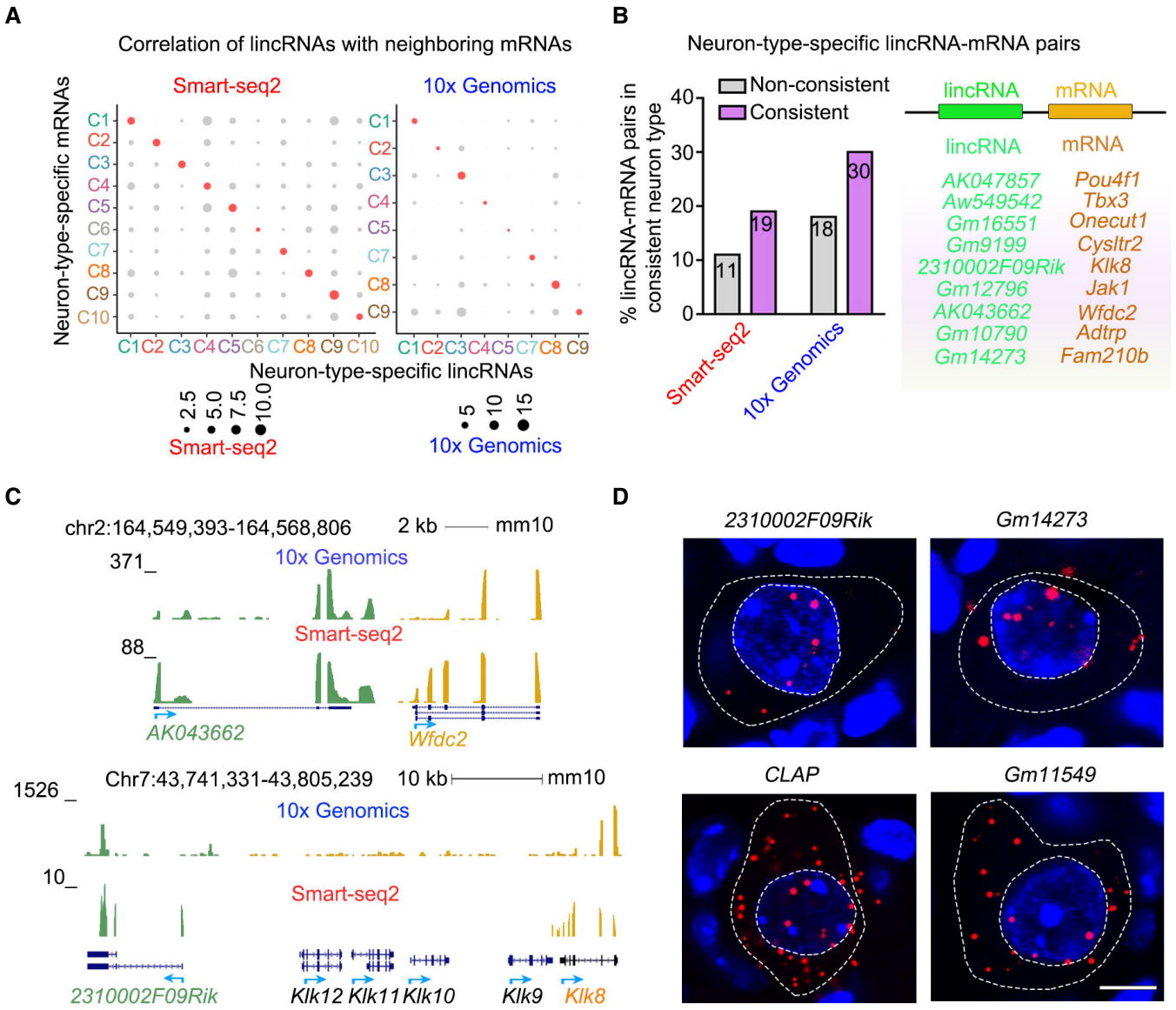


**Figure 4. Coexpression of neuron-type-specific lincRNAs with neighboring mRNAs.**

A Dot plot showed that the highly neuron-type-specific lincRNAs and their adjacent protein-coding genes were more likely to predominantly express in the same neuron type by both Smart-seq2 and 10× Genomics.

B Statistical results showed that the percentage of consistent lincRNA-mRNA pairs were higher than that of those non-consistent pairs in both Smart-seq2 and 10× Genomics. Top-ranking list of lincRNA-mRNA pairs is showing at right.

C scRNA-seq coverage showed that C3-type-specific *AK043662* is genomically adjacent to *Wfdc2* (Upper) and C5-type-specific *2310002F09Rik* is genomically adjacent to *Klk8* (Bottom).

D Representative smFISH images in DRG sections and quantitative results showed that *2310002F09Rik* and *Gm14273* were more enriched in the nucleus, whereas *CLAP* and *Gm11549* were mainly distributed in the cytoplasm. DAPI served as a nuclear marker. Scale bar, 10 μm.

was also significantly higher than those of mRNAs (Fig EV2D). All these results suggest a highly neuron-type-specific expression of lincRNAs in DRG neurons.

### A landscape of neuron-type-specific lincRNAs is established in somatosensory neurons

In total, about 200 neuron-type-specific lincRNAs (SPM ≥ 0.8, TPM ≥ 1) were annotated by 10× Genomics (58 lincRNAs) and/or Smart-seq2 (172 lincRNAs), with 30 overlapped ones reported by two methods (Figs 3A and B, EV3A; Dataset EV2). The 142 lincRNAs were uniquely identified by Smart-seq2 (Fig EV3B) owing to higher sequencing depths and 28 lincRNAs were solely detected by 10× Genomics (Fig EV3C; Dataset EV3) owing to more captured cells. Furthermore, 11 of 28 lincRNAs specially identified in 10× Genomics were found in the subtypes of DRG neurons (Fig EV3D). Meanwhile, about 60% of 200 lincRNAs were distributed across three neuron types including C2 (*Nppb*$^{+}$, 19.5%),

 

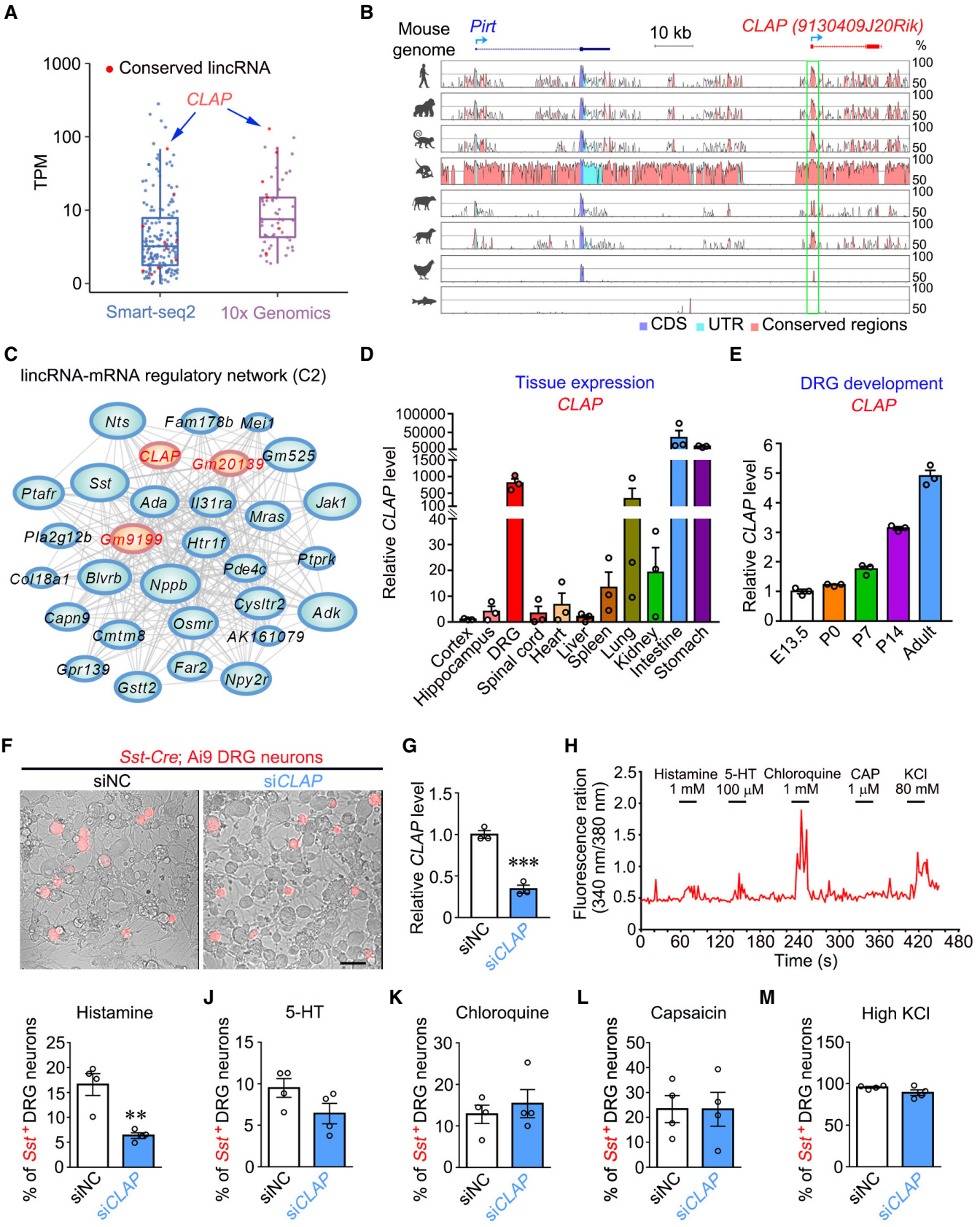
A
Conserved lincRNA
CLAP
TPM
1000
100
10
0
Smart-seq2
10x Genomics
B
Mouse genome
Pirt
10 kb
CLAP (9130409J20Rik)
%
100
50
CDS
UTR
Conserved regions
C
lincRNA-mRNA regulatory network (C2)
Nts
Fam178b
Mei1
CLAP
Gm20139
Gm525
Sst
Ptafr
Ada
Il31ra
Jak1
Mras
Pla2g12b
Gm9199
Htr1f
Ptprk
Col18a1
Blvrb
Nppb
Pde4c
Cysltr2
Adk
Capn9
Osmr
Cmtm8
AK161079
Gpr139
Far2
Gstt2
Npy2r
D
Tissue expression
CLAP
Relative CLAP level
100000
50000
5000
1500
1000
500
100
40
30
20
10
0
Cortex
Hippocampus
DRG
Spinal cord
Heart
Liver
Spleen
Lung
Kidney
Intestine
Stomach
E
DRG development
CLAP
Relative CLAP level
6
5
4
3
2
1
0
E13.5
P0
P7
P14
Adult
F
Sst-Cre; Ai9 DRG neurons
siNC
siCLAP
G
Relative CLAP level
1.5
1.0
0.5
0
***
siNC
siCLAP
H
Histamine 1 mM
5-HT 100 μM
Chloroquine 1 mM
CAP 1 μM
KCl 80 mM
Fluorescence ration (340 nm/380 nm)
2.5
2.0
1.5
1.0
0.5
0
0
60
120
180
240
300
360
420
480
Time (s)
I
Histamine
% of Sst+ DRG neurons
25
20
15
10
5
0
**
siNC
siCLAP
J
5-HT
% of Sst+ DRG neurons
15
10
5
0
siNC
siCLAP
K
Chloroquine
% of Sst+ DRG neurons
30
20
10
0
siNC
siCLAP
L
Capsaicin
% of Sst+ DRG neurons
50
40
30
20
10
0
siNC
siCLAP
M
High KCl
% of Sst+ DRG neurons
150
100
50
0
siNC
siCLAP

**Figure 5.**

**Figure 5. *CLAP* is highly conserved and abundantly expressed in C2 type of DRG neurons.**

A Boxplot showing the abundance of highly expressed neuron-type-specific lincRNAs in Smart-seq2 and 10× Genomics. Each dot represents a lincRNA, colored (Red) by its conservation between mouse and human. In boxplot, central band, boxes, and whiskers represent median value, second/third quartiles and minimum/maximum value to second/third quartiles, respectively.

B Sequence conservation analysis of lincRNA *CLAP* and upstream mRNA *Pirt* in 9 different species including mouse, human, chimpanzee, rhesus monkey, rat, cow, dog, chicken, and zebrafish, which were visualized with the VISTA browser. CDS, coding sequence. UTR, untranslated region.

C Gene co-expression network identified by WGCNA shows that *CLAP* co-expressed with known marker genes such as *Sst* and *Nppb* in C2-type neurons. Blue and red colors represent mRNAs and lincRNAs, respectively.

D qPCR showed that *CLAP* was highly expressed in the DRG and other visceral organs such as small intestine, stomach, and lung. The results are presented as mean ± SEM ($n = 3$).

E qPCR showed that the expression of *CLAP* was gradually increased from E13.5 to adult DRGs. The results are presented as mean ± SEM ($n = 3$).

F Representative bright-field and fluorescent images showing the *Sst-cre*; Ai9 neurons for calcium imaging following si*CLAP* transfection. Scale bar, 10 μm.

G qPCR showed that the expression of *CLAP* was decreased by siRNA treatment in cultured *Sst-Cre*; Ai9 DRG neurons. $n = 3$. $^{**}P < 0.01$ versus siNC.

H Traces showed that a *Sst-Cre*; Ai9 tdTomato neuron was evoked by histamine (1 mM), 5-HT (100 μM), chloroquine (1 mM), capsaicin (CAP, 1 μM), and KCl (80 mM) in the calcium imaging.

I–M The percentage of *Sst-Cre*; Ai9 neurons evoked by histamine (I) was decreased by knockdown of *CLAP*, whereas the percentage of these neurons affected by 5-HT (J), chloroquine (K), capsaicin (L), and KCl (M) were not changed. $n = 4$. $^{**}P < 0.01$ versus siNC.

Data information: (G, I, J, K, L and M) The results are presented as mean ± SEM ($n = 4$). Unpaired *t*-test was used for all statistical analyses.

C3 ($Th^+/Slc17a8^+$, 18.5%) and C9 ($S100b^+/Baiap2l1^+$, 13.5%; Fig 3C), which were previously suggested to play roles in thermal, itch and mechanical sensation (Li *et al*, 2016; Zheng *et al*, 2019). Additionally, we also performed *de novo* assembly of transcripts and filtered novel lincRNAs using full-length Smart-seq2 datasets. Total 2,456 novel lincRNAs were found, 1,222 of which were also detected in our 10× Genomics datasets (Fig EV4A). Moreover, 42 novel lincRNAs were found to be cell-type-specific in DRG neurons based on their high expression specificity (Fig EV4B). Among them, *MSTRG.70926*, *MSTRG.113954*, and *MSTRG.51119* were specifically expressed in C2 (Fig EV4C), C3 (Fig EV4D) and C5 (Fig EV4E) types, respectively.

Next, we applied robust rank aggregation (RRA) method (Kolde *et al*, 2012) to evaluate the abundances and specificities of those 200 annotated neuron-type-specific lincRNAs (Fig 3D; Dataset EV2). Among top-ranked lincRNAs, the abundances of *AK047857*, *9130409J20Rik* (*CLAP*), *Gm11549*, *0610043K17Rik*, *2310002F09Rik*, and *C530044C16Rik* were 10 times higher than those in other types (Fig EV5A–E), and their SPMs were also much higher than those of other lincRNAs (Fig EV5F). We then set to validate the high-ranking lincRNAs in dissociated DRG neurons (Fig 3D; Appendix Fig S1A). Single-cell reverse transcription PCR (RT–PCR) showed exclusive distribution of these lincRNAs in specific types of DRG neurons expressing marker genes (Appendix Fig S1B). For example, *C530044C16Rik* was highly expressed in the $Gal^+$ neurons (C1), but not in the $Nppb^+$ neurons (C2). In contrast, *0610043k17Rik* was specifically localized in the $Nppb^+$ neurons, but rarely expressed in the $Gal^+$ neurons (Appendix Fig S1C). In addition, *2310002F09Rik* was exclusively expressed in the $Mrgprd^+$ neurons (C5), whereas *Gm11549* was relatively enriched in the $Th^+$ neurons (C3; Appendix Fig S1D).

To further confirm cellular localization of these lincRNAs *in vivo*, we carried out single-molecular fluorescent *in situ* hybridization (smFISH) by utilizing distinct cell-type-specific marker genes expressing *Cre*-driven tdTomato reporter of Ai9 mice (Madisen *et al*, 2010). smFISH showed that *C530044C16Rik* was mainly expressed in the $Gal^+$ neurons (Fig 3E), but rarely distributed in $Sst^+$, $Slc17a8^+$ (*Slc17a8* as a C3 type marker) and $Mrgprd^+$ neurons from L4/5 DRG section of mice (Fig 3E; Appendix Fig S1E). More importantly, the proportion of *C530044C16Rik* in $Gal^+$ and $Sst^+$ neurons were consistent with that from the 10× Genomics data (Fig 3E). Meanwhile, similar to the 10× Genomics results, *CLAP* was found to be specifically localized in the $Sst^+$ neurons, but rarely expressed in the $Gal^+$ (Fig 3F) and $Slc17a8^+$ as well as $Mrgprd^+$ DRG neurons (Appendix Fig S1F), suggesting a highly C2-type-specific lincRNA. Additionally, *Gm11549* was highly localized in the $Slc17a8^+$ neurons, whereas *2310002F09Rik* was specially distributed in the $Mrgprd^+$ neurons (Fig 3G and H; Appendix Fig S1G and H). Furthermore, we performed double smFISH to assess the co-localization of those neuron-type-specific lincRNAs. Substantially, *C530044C16Rik*, *CLAP*, and *Gm11549* were rarely co-localized with *2310002F09Rik* in DRG neurons (Fig 3I–K), further suggesting the enrichment of these lincRNAs in specific types of somatosensory neurons. Taken together, a landscape of neuron-type-specific lincRNAs is established in somatosensory neurons.

## lincRNAs are coexpressed with neighbor mRNAs in a neuron-type-specific manner

lncRNAs have been shown to likely coexpress with their divergent neighboring genes in distinct types of cells (Ulitsky & Bartel, 2013; Briggs *et al*, 2015). We then evaluated the possible expression correlation of neuron-type-specific lincRNAs with their nearby protein-coding genes within 50 kb in genome. As expected, neuron-type-specific lincRNAs and their adjacent protein-coding genes were predominantly expressed in the same type of neurons (Fig 4A). The percentage of highly neuron-type-specific lincRNAs (SPM ≥ 0.8) and their neighboring mRNAs (10× Genomics, 30%; Smart-seq2, 19%) was higher than that of non-specific lincRNA-mRNA pairs (SPM < 0.5, 10× Genomics, 18%; Smart-seq2, 11%; Fig 4B). Intriguingly, these top-ranked mRNAs consist most of the transcription factors such as POU 4 Class 4 Homeobox 1 (*Pou4f1*) and T-Box transcription factor 3 (*Tbx3*) as well as pain or itch-related genes including Cysteinyl leukotriene receptor 2 (*Cysltr2*), Janus kinase 1 (*Jak1*), and Kallikrein-8 (*Klk8*), implying the potential functions of neighbor lincRNAs in the specification and sensory transmission of DRG neurons. For instance, *AK047857* and *AK043662*, C3-type-specific lincRNAs, were localized in the genomic position

 

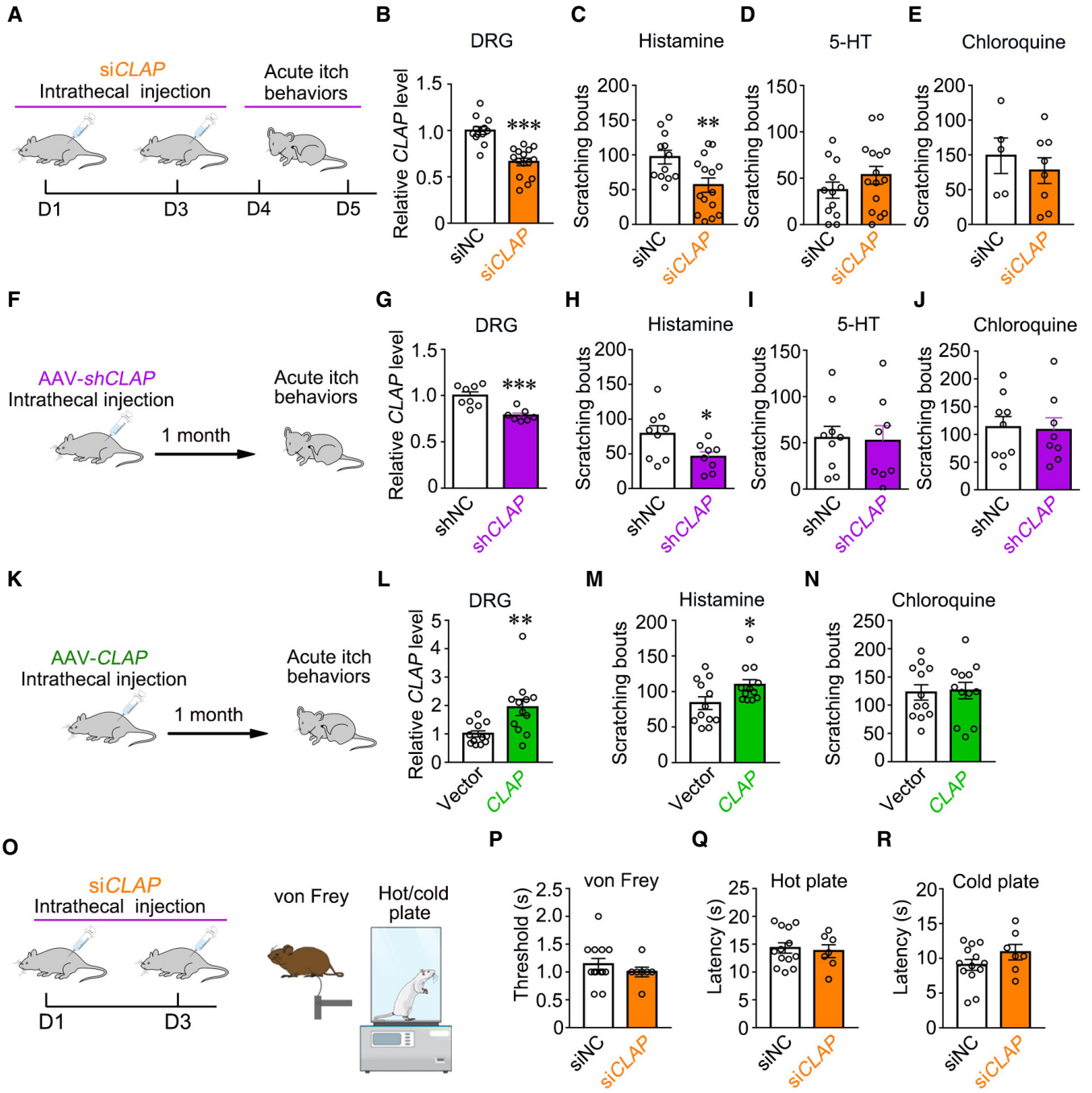


**Figure 6.**

near C3-type-enriched *Pou4f1 and Wfdc2*, respectively (Fig 4C; Appendix Fig S2A–C). Of note, *Pou4f1* mRNA gene has been reported as a critical transcription factor in subtype specification of DRG neurons (Zou *et al*, 2012), implying a potential role of its paired lincRNA *AK047857*. Additionally, *2310002F09Rik*, a C5-subtype-specific lincRNA, was genomically adjacent to the kallikrein (KLK) family *Klk8* gene (Fig 4C; Appendix Fig S2D), which have been suggested to play an important role in itch sensation (Mack & Kim, 2018). Thus, this coexpression pattern of neuron-type-specific lincRNAs with their adjacent mRNAs suggests their regulatory potential in somatosensory neurons.

Subcellular localization of lincRNAs implies their roles in distinct cellular processes (Chen, 2016; Carlevaro-Fita & Johnson, 2019). A few well-characterized lincRNAs such as *Air* and *Kcna1ot1* have been suggested to act as a *cis* transcriptional regulator on its neighbored coding genes and mainly localized in the nucleus (Chen, 2016; Carlevaro-Fita & Johnson, 2019). Then, we determined the subcellular localization of those paired lincRNAs by morphological assay.

**Figure 6. *CLAP* is sufficient for histamine-induced scratching.**

A Research flowchart for acute itch behavioral test following intrathecal injection of siRNA in mice. Before acute itch behavior testing, mice were intrathecally injected with siRNA 2 times in 3 days.

B qPCR showed that the *CLAP* level was significantly decreased by si*CLAP* in the DRG following intrathecal injection. The results are presented as mean ± SEM (siNC = 12, si*CLAP* = 15). ***$P < 0.001$ versus siNC.

C–E Knockdown of *CLAP* reduced itch scratching evoked by histamine (C), but not 5-HT (D) and chloroquine (E). The results are presented as mean ± SEM (For histamine and 5-HT, siNC = 12, si*CLAP* = 15; for chloroquine, siNC = 5, si*CLAP* = 8). **$P < 0.01$ versus siNC.

F Research flowchart for AAV-mediated knockdown of *CLAP* by intrathecal injection of AAV-sh*CLAP*-GFP.

G qPCR showed that the *CLAP* level was significantly decreased by AAV-sh*CLAP*-GFP in DRGs following intrathecal injection and testing of acute itch behavior. The results are presented as mean ± SEM (shNC, $n = 8$; sh*CLAP*, $n = 7$). ***$P < 0.001$ versus shNC.

H–J Knockdown of *CLAP* reduced the scratching induced by histamine (H), but not that by 5-HT (I) and chloroquine (J). The results are presented as mean ± SEM (shNC, $n = 9$; sh*CLAP*, $n = 8$). *$P < 0.05$ versus shNC.

K Research flowchart for AAV-mediated overexpression of *CLAP* by intrathecal injection of AAV-*CLAP*.

L qPCR showed that the *CLAP* level was significantly increased by AAV-*CLAP* in DRGs following intrathecal injection. The results are presented as mean ± SEM ($n = 12$). **$P < 0.05$ versus vector.

M, N Overexpression of *CLAP* increased the scratching induced by histamine (M), but not that by chloroquine (N). The results are presented as mean ± SEM ($n = 12$). *$P < 0.05$ versus vector.

O Flowchart for mechanical, hot, and cold behavioral tests following intrathecal injection of siRNA in mice.

P–R The threshold for mechanical (P), heat (Q) and cold (R) responses were not affected by knockdown of *CLAP*. The results are presented as mean ± SEM (siNC, $n = 13$; si*CLAP*, $n = 7$).

Data information: Unpaired *t*-test was used for all statistical analyses.

Interestingly, smFISH of L4/5 DRG sections of adult mice exhibited that the paired lincRNAs such as *2310002F09Rik* and *Gm12473* were more enriched in the nucleus (Fig 4D), whereas those non-paired lincRNAs including *CLAP* and *Gm11549* exhibited stronger cytoplasmic distribution, and their neighboring genes consisted of *Pirt* (*CLAP*) and *Exosc9* (*Gm11549*) without displaying neuron-type specificity (Appendix Fig S2E and F), implying a possibly post-transcriptional role in DRG neurons. Furthermore, to confirm the *cis* regulatory role of nuclear-enriched lincRNA such as *2310002F09Rik*, we performed siRNA-mediated knockdown experiments in cultured DRG neurons. qPCR detected that si*2310002F09Rik* significantly reduced the mRNA level of *KLK8*, further implying a *cis*-regulatory role of *2310002F09Rik* (Appendix Fig S2G). Taken together, combining scRNA-seq and subcellular localization analysis, several nuclear-enriched and type-specific lincRNAs are identified and supposed to be with *cis* regulatory role on the neighboring gene expression.

### *CLAP* is conserved and abundantly expressed in C2-type DRG neurons

The majority of these conserved lincRNAs among different species have been suggested to serve as the functional regulators in different biological processes (Ulitsky, 2016). To screen the neuron-type-specific lincRNAs that potentially function in sensory transmission, we analyzed the conservation of lincRNAs between human and mouse. According to the principal of sequence and position conservation, 14 neuron-type-specific lincRNAs were identified from 230 mouse annotated conserved lincRNAs in the DRG based on the data from two scRNA-seq methods (Appendix Fig S3A and B). Among 14 lincRNAs, *CLAP* and *Gm16551*, which were highly expressed in C2 (*Nppb*$^+$) and C7 (*S100b*/*Wnt7a*$^+$) type of DRG neurons, respectively, were identified consistently in both two scRNA-seq methods (Appendix Fig S3B and C). Remarkably, the analysis of DRG cells from 10× Genomics further revealed that *CLAP* was almost exclusively expressed in the neurons but not other cells (Appendix Fig S3D). Combined the abundance and conservation among those highly neuron-type-specific lincRNAs, *CLAP* was suggested as the most conserved and abundant lincRNA among 200 neuron-type-specific lincRNAs (Fig 5A), subject to following functional study.

Further analysis of the genomic localization of *CLAP* showed that the first exon of *CLAP* exhibited high similarity throughout 8 species (Fig 5B). Importantly, RT–PCR showed that *CLAP* was also detected in human DRG (Appendix Fig S3E), suggesting the conserved expression of *CLAP* between human and mouse. More importantly, the lincRNA-mRNA regulatory network performed by weighted gene coexpression network analysis (WGCNA) showed that *CLAP* was involved in those gene modules highly related to the activity of neuropeptide receptor, which comprised of several itch or pain-related genes such as *Sst* and *Nppb* specifically expressing in C2-type neurons (Fig 5C; Appendix Fig S4A and B). Combined the results from single-cell RT-PCR, smFISH, Smart-seq2, and 10× Genomics (Figs 3F and EV5B and F; Appendix Fig S1B), *CLAP* was highly and specifically expressed in the C2-type DRG neurons.

Both bulk RNA-seq for DRGs and scRNA-seq for DRG neurons exhibited the absent sequence at the 5′ and 3′ distal region of known *CLAP* annotation (Appendix Fig S5A). Then, we performed 5′RACE and 3′RACE to reveal the full-length sequence of *CLAP* as 2,166 nt, perfectly matched with the mapped signals by scRNA-seq (Appendix Fig S5A). Analysis with Coding Potential Calculator 2 (CPC2) and Coding Potential Alignment Tool (CPAT) softwares showed that *CLAP* did not have a coding ability like other known lncRNAs, such as *GAS5*, *H19*, and *HOTAIR* (Appendix Fig S5B). To further exclude the coding potential of *CLAP*, we examined the expression of the predicated open reading frame (ORF) within the conserved region (First exon) of *CLAP* by inserting three continuous Flag tags in the middle region or after the start codon and before the stop codon of ORF in HEK293 cells (Appendix Fig S5C). Although RT–PCR showed that the exogenous *CLAP* level were comparable between those constructs, immunoblotting of Flag did not reveal any protein band (Appendix Fig S5D), suggesting lack of coding potential with *CLAP*.

Quantification of smFISH images in DRG neurons exhibited that *CLAP* was more enriched in the cytoplasm than in the nucleus (Appendix Fig S2E). qPCR showed that *CLAP* was highly expressed

 

in DRGs but not in other tissues from central nervous system such as cortex, hippocampus, and spinal cord (Fig 5D). Interestingly, *CLAP* was also highly expressed in the visceral organs such as small intestine, stomach and lung (Fig 5D). Furthermore, qPCR showed that the developmental expression of *CLAP* was gradually increased from E13.5 to adult stage (Fig 5E). The spatial and temporal expression pattern raises a possibility that *CLAP* mainly functions in somatosensory transmission. Taken together, these data indicate that *CLAP* is a highly conserved and abundant lincRNA specifically expressed in C2-type neurons, implying its potential connection to sensory transmission.

### *CLAP* knockdown decreases histamine-induced neuronal excitability

Previous study and transcriptome analysis revealed that the function of C2-type ($Sst^+$) neurons is highly associated with chemical-induced pruritus including histamine, 5-hydroxytryptamine (5-HT), chloroquine (CQ), and TPRV1-mediated heat response (Li *et al*, 2016; Stantcheva *et al*, 2016; Huang *et al*, 2018; Solinski *et al*, 2019). To obtain *CLAP*-enriched C2-type neurons for further functional study, we performed fluorescent activating cell sorting (FACS) to purify specific neuronal type of somatosensory neurons. *Cre*-driven by Nav1.8 promoter (*SNS-Cre*) and *Sst-Cre*; Ai9-tdTomato mice were carried out to label the majority of DRG neurons and C2-type neurons, respectively (Appendix Fig S5E). Bright-field and fluorescent images showed that FACS-obtained neurons were almost $tdTomato^+$ (Appendix Fig S5F). qPCR detected that *Nppb* as well as *CLAP* were highly enriched in the neurons derived from *Sst*-Cre; Ai9 mice, compared to that from *SNS-Cre*; Ai9 mice (Appendix Fig S5G). Meanwhile, other type-specific lincRNAs such as *Gm11549* and *2310002F09Rik* as well as other type-specific markers including *Th and Mrgprd* were relatively low in *Sst-Cre*; Ai9 neurons (Appendix Fig S5G). Thus, *CLAP* is enriched in cultured $Sst^+$ DRG neurons.

To investigate the potential cellular functions of *CLAP* in C2-type neurons, we performed calcium imaging after application of small interfering (si)RNA to downregulate *CLAP* in cultured *Sst-Cre*; Ai9 DRG neurons (Fig 5F). qPCR and smFISH showed that the expression level of *CLAP* was downregulated by si*CLAP* in *Sst-Cre*; Ai9 DRG neurons (Fig 5G; Appendix Fig S6A). Calcium imaging showed that the calcium influx of *Sst-Cre*; Ai9 neurons was induced by application of distinct pruritogens including histamine, 5-HT, CQ and capsaicin (Fig 5H). Furthermore, *CLAP* knockdown significantly reduced the percentage of neurons activated by 1 mM histamine from *Sst-Cre*; Ai9 mice (Fig 5I), whereas did not influence the percentage of neurons induced by 100 μM 5-HT or 1 mM CQ (Fig 5J and K), suggesting a histamine-dependent effect operated by *CLAP*. TRPV1 has been reported to contribute to itch and pain signal transduction (Dong & Dong, 2018). However, calcium imaging showed that the percentage of neurons activated by 1 μM capsaicin, an agonist of TRPV1 as previously reported (Han *et al*, 2013; Yang *et al*, 2017), was not affected in *Sst-Cre*; Ai9 mice (Fig 5L). Equivalent response induced by 80 mM KCl between control and *CLAP* knockdown excluded the possible change of neuronal excitability (Fig 5M). Additionally, the amplitude of calcium influx induced by histamine, 5-HT, chloroquine, and capsaicin was not affected by *CLAP* knockdown (Appendix Fig S6B–E). Therefore, *CLAP* is selectively involved in histamine-mediated activation of $Sst^+$ DRG neurons.

### *In vivo* regulation of *CLAP* affects histamine-induced itch

To determine the *in vivo* function of *CLAP* in acute itch transmission, we examined scratching behavior of mice by intradermal injection of distinct pruritogens after 2-time intrathecal injections of siRNA (Fig 6A). qPCR detected that endogenous *CLAP* was efficiently reduced by si*CLAP* in lumbar 4/5 (L4/5) DRGs (Fig 6B). Importantly, downregulation of *CLAP* significantly reduced the histamine-induced scratching (Fig 6C), whereas did not affect the 5-HT and CQ-induced scratching (Fig 6D and E). At the same time, we also carried out AAV-mediated short hairpin (sh)RNA to reduce *CLAP* level in DRGs (Appendix Fig S7A). qPCR detected that *CLAP* was dramatically reduced by AAV-sh*CLAP* after 7-day infection in cultured DRG neurons (Appendix Fig S7B and C). After 1 month of intrathecal injection with AAV-sh*CLAP* (Fig 6F), endogenous *CLAP* was moderately reduced by sh*CLAP* in L4/5 DRGs (Fig 6G). Subsequently, acute itch behavioral test showed that the histamine-induced scratching was significantly reduced (Fig 6H), while 5-HT and CQ-induced scratching remained unchanged (Fig 6I and J). Although the efficiency for siRNA- or AAV-mediated *CLAP* knockdown was relatively lower *in vivo* than that *in vitro*, both *CLAP* knockdown induced the significant decrease of histamine-induced scratching. We speculated that the long-term infection of AAV might have accumulative effects (more than 1 month) to produce the similar itch behavior with short-term infection of siRNA (5 days) even with a relatively low knockdown efficiency. Moreover, the fact that relatively mild reduction in *CLAP in vivo* could lead to an obvious phenotype suggests an important role of *CLAP* in itch regulation and further indicates that *CLAP* may affect critical molecules.

To verify whether *CLAP* is sufficient for histamine-induced scratching, we performed intrathecal injection of AAV-mediated overexpression of *CLAP* (Fig 6K). qPCR detected that infection of AAV-*CLAP* significantly increased the expression of *CLAP* in L4/5 DRG (Fig 6L). Meanwhile, overexpression of *CLAP* increased histamine-induced scratching (Fig 6M), whereas did not affect CQ-induced scratching (Fig 6N), implying that *CLAP* is sufficient for histamine-induced itch. Additionally, downregulation of *CLAP* did not affect IL-31-induced scratching (Appendix Fig S7D–F), implying that *CLAP* is not involved in the IL-31-induced itch. Therefore, both *in vivo* knockdown and overexpression results suggest a role of *CLAP* selectively involved in the histamine-dependent itch.

At the same time, we performed von Frey assay and hot/cold plate following intrathecal injection of si*CLAP* to determine whether other somatosensory behaviors were affected by *CLAP* downregulation (Fig 6O). In fact, the mechanical threshold, and thermal and cold withdrawal thresholds were not affected by *CLAP* downregulation (Fig 6P–R). These results suggest that C2-specific lincRNA *CLAP* regulates histamine-dependent itch.

### *CLAP* regulates itch-related gene expression partially via the regulatory role of MSI2

To explore the underlying mechanism of *CLAP* in regulating neuronal excitability and itch, we performed RNA-seq to find out potentially regulated genes in the L4/L5 DRGs of those mice following

intrathecal injection of si*CLAP* and acute itch behavioral test (Fig 7A). RNA-seq results from siNC and si*CLAP* showed that *CLAP* was significantly reduced in DRGs (Fig 7B). Analysis of differential gene expression revealed that *CLAP* knockdown caused 318 upregulated and 549 downregulated genes, respectively (Fig 7C; Dataset EV4), which further implicated that those regulated gene modules were highly enriched in the receptor and ion channel signaling pathways (Appendix Fig S8A). More importantly, *CLAP* knockdown especially downregulated several C2-specific genes including *Sst*, *Gm525*, Platelet-activating factor receptor (*Ptafr*), *Cysltr2*, Sphingosine-1-phosphate receptor 1 (*S1pr1*), and Oncostatin M receptor (*Osmr*), and most of them were associated with cytokine receptor signaling (Fig 7C and D; Appendix Fig S8B and C). Despite without affecting the mRNA level of histamine receptor H1 (*Hrh1*), *CLAP* knockdown significantly reduced the expression of phospholipase C β3 subunit (*Plcb3*; Fig 7D) that mediates histamine-induced scratching behavior (Han *et al*, 2006). Additionally, the mRNA levels of other itch-related ion channels such as *Trpa1* and *Trpv1* as well as *Pirt*, the neighboring gene of *CLAP*, were not affected by si*CLAP* (Fig 7D; Appendix Fig S8D). Furthermore, qPCR confirmed that the mRNA levels of *Sst*, *Plcb3*, *and Cysltr2* were significantly decreased in L4/5 DRGs of mice following intrathecal injection of si*CLAP* (Appendix Fig S8E). To exclude the off-target effects by siRNA, we performed intrathecal injection with AAV-mediated expression siRNA-resistant *CLAP* (*CLAP*$^{R}$) to rescue si*CLAP*-induced effects. After over one-month intrathecal injection of *CLAP*$^{R}$, we performed two-time intrathecal injections of siRNA and detected gene expression (Fig 7E). qPCR detected that *CLAP* was fully rescued by overexpression of *CLAP*$^{R}$ (Fig 7F). Meanwhile, downregulated C2-specific genes including *Sst*, *Plcb3*, and *Cysltr2* by si*CLAP* were fully rescued by *CLAP*$^{R}$ in L4/5 DRGs of mice (Fig 7F), excluding the potential off-target effects of *CLAP*. Taken together, *CLAP* regulates the expression of several itch-related genes, especially C2-type-specific genes in DRG neurons.

Previous studies report that largely cytoplasm-enriched lincRNAs perform diverse functions by directly interacting with RNA-binding proteins (RBPs; Yao *et al*, 2019). To investigate the regulatory mechanism of *CLAP*, we firstly analyzed the POSTAR2 database, which contains > 1,200 cross-linking immunoprecipitation followed by high-throughput sequencing (CLIP-seq) datasets from various species and tissues, to search for potential RBPs in binding *CLAP* and involving in *CLAP*-mediated functions. Interestingly, we found that Mosashi RNA binding Protein 2 (MSI2), previously reported to regulate mRNA decay (Bennett *et al*, 2016; Zou *et al*, 2022), was identified to specifically binds *CLAP* in mouse intestinal epithelium (Appendix Fig S9A and B). Meanwhile, based on the MSI2-binding RNAs and *CLAP*-regulated genes, we found that *Plcb3* was likely regulated by cooperation of *CLAP* and MSI2. RNA immunoprecipitation in mouse DRGs also confirmed the interaction between MSI2 and *CLAP* in mouse DRG (Fig 7G).

To address whether MSI2 was involved in the *CLAP*-regulated *Plcb3* expression, we firstly confirmed the knockdown efficiency of siRNA targeting to MSI2 (Appendix Fig S9C and D) and performed intrathecal injection of si*CLAP* and si*MSI2* (Fig 7H). qPCR detected that *CLAP* and *Msi2* were significantly reduced by si*CLAP* or/and si*MSI2* after 2-time intrathecal injections of siRNA, respectively (Fig 7I). Importantly, the decreased level of *Plcb3* by si*CLAP* was completely rescued by knockdown of MSI2, indicating an important role of MSI2 in the *CLAP*-regulated *Plcb3* expression (Fig 7I). At the same time, other C2-type-specific gene such as *Sst* was not detected to associate with MSI2 (Fig 7G), implying roles of other molecules in *CLAP*-mediated regulation besides MSI2. Taken together, these data suggest that *CLAP* regulates itch-related gene expression partially via the regulatory role of MSI2.

## Discussion

Somatosensory transmission relies on distinct types of sensory neurons activated by mechanical, thermal, and chemical stimuli (Basbaum *et al*, 2009). In the present study, by re-analyzing our scRNA-seq datasets of recently published 10× Genomics together with previously published Smart-seq2, we determine the distribution of lincRNAs in DRG cells and reveal that lincRNAs are preferably enriched in somatosensory neurons and exhibit higher type specificity than coding genes. Furthermore, we uncover the landscape of neuron-type-specific lincRNAs at single-cell resolution by integrating the data from two scRNA-seq methods. Importantly, we characterize a conserved and previously underappreciated lincRNA *CLAP* that functionally contributes to histamine-mediated itch transmission possibly through downregulating the expression of type-specific and itch-associated genes. Our datasets remarkably address differential and specific distribution of lincRNAs in distinct types of somatosensory neurons and greatly advance the understanding of regulatory roles of lincRNAs in somatosensory transmission with a neuron-type-dependent manner.

### Profiling a landscape of neuron-type-specific lincRNAs in somatosensory neurons

Technologies of scRNA-seq have been recently advanced in numerous studies (Olsen & Baryawno, 2018). Smart-seq2 empowers in-depth high-coverage RNA-seq but usually only detects a small range of cells because of high costs, whereas 10× Genomics captures more cells but detects fewer genes (Ziegenhain *et al*, 2017). For Smart-seq2, we classified sensory neuron into 10 types and 14 subtypes by combining high-coverage sequencing and hierarchical clustering based on neuron size (Li *et al*, 2016), showing inconsistent neuron subtypes and marker genes with previous study (Usoskin *et al*, 2015) due to low-coverage sequencing and limited number of genes tested. In our study, the clustering for 10× Genomics analysis is consistent with the recent study (Zeisel *et al*, 2018). Therefore, comprehensive analysis by integrating two scRNA-seq technologies is a preferred approach to investigate the landscape, as recent studies well applied in analyzing human immune cells (Stuart *et al*, 2019; Zhang *et al*, 2019). Despite lincRNA exhibiting highly tissue specificity (Ransohoff *et al*, 2018), it is still unknown whether lincRNAs display cell-type specificity at single-cell level especially for the neurons, due to their extremely lower expression than mRNA (Liu *et al*, 2016). Combing analysis of SPM and CV for individual gene in single cell, our study revealed that lincRNAs exhibited higher specificity and heterogeneity than coding genes in distinct types and subtypes of somatosensory neurons, facilitating the understanding of lincRNA specificity not only in tissue but also within one type of cells. Additionally, both Smart-seq2 and 10× Genomics likely have the limitations in

 

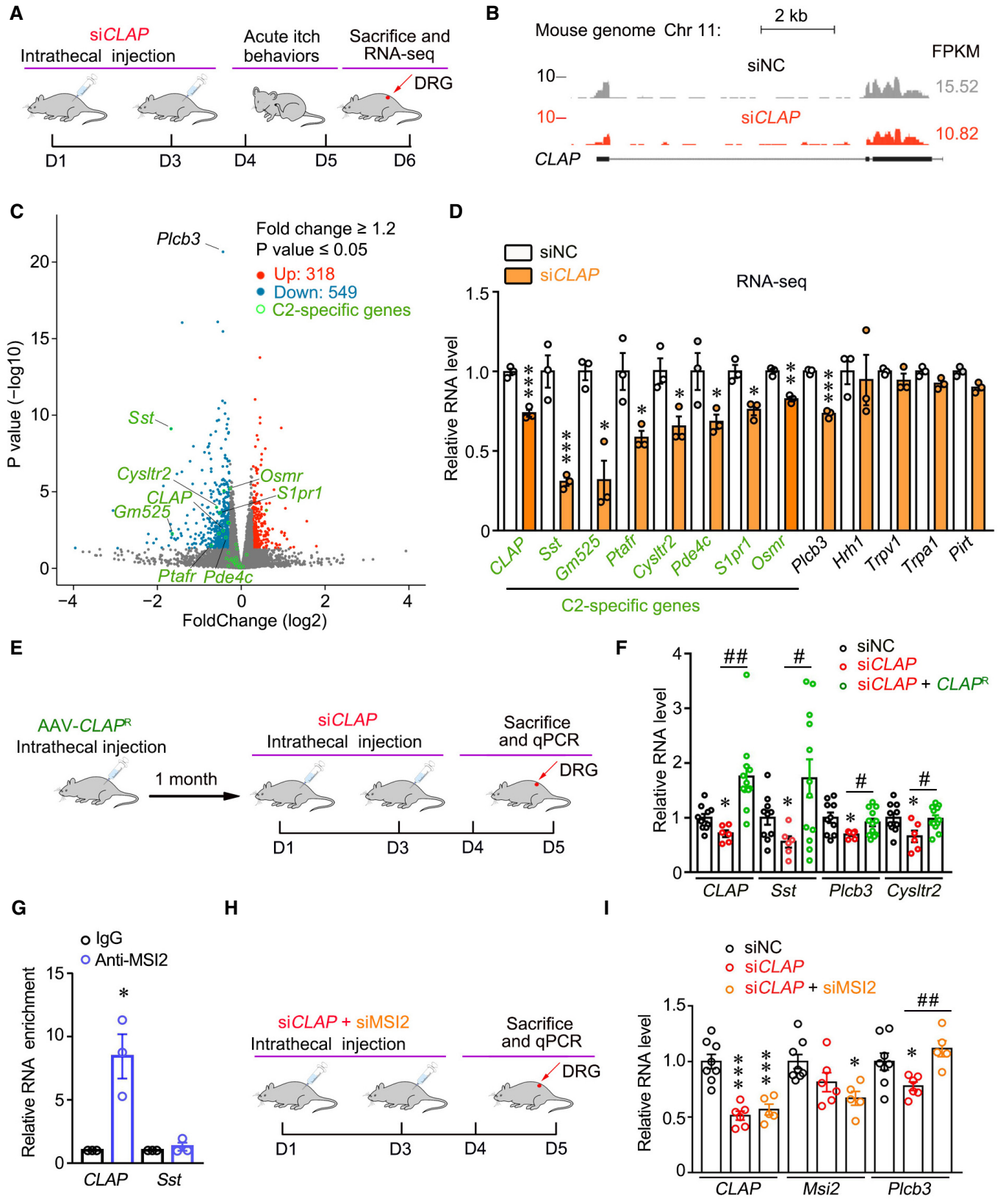
A
siCLAP
Intrathecal injection
Acute itch behaviors
Sacrifice and RNA-seq
DRG
D1
D3
D4
D5
D6
B
Mouse genome Chr 11:
2 kb
FPKM
siNC
15.52
siCLAP
10.82
CLAP
C
Fold change ≥ 1.2
P value ≤ 0.05
Up: 318
Down: 549
C2-specific genes
Plcb3
Sst
Cysltr2
Osmr
S1pr1
CLAP
Gm525
Ptafr
Pde4c
P value (−log10)
FoldChange (log2)
D
siNC
siCLAP
RNA-seq
Relative RNA level
CLAP
Sst
Gm525
Ptafr
Cysltr2
Pde4c
S1pr1
Osmr
Plcb3
Hrh1
Trpv1
Trpa1
Pirt
C2-specific genes
E
AAV-CLAPR
Intrathecal injection
1 month
siCLAP
Intrathecal injection
Sacrifice and qPCR
DRG
D1
D3
D4
D5
F
siNC
siCLAP
siCLAP + CLAPR
Relative RNA level
CLAP
Sst
Plcb3
Cysltr2
G
IgG
Anti-MSI2
Relative RNA enrichment
CLAP
Sst
H
siCLAP + siMSI2
Intrathecal injection
Sacrifice and qPCR
DRG
D1
D3
D4
D5
I
siNC
siCLAP
siCLAP + siMSI2
Relative RNA level
CLAP
Msi2
Plcb3

**Figure 7.**

**Figure 7. *CLAP* regulates itch-related gene expression by partially through the regulatory role of MSI2.**

A Research flowchart for RNA-seq of DRGs following intrathecal injection.

B Visualization of knockdown efficiency of *CLAP* in RNA-seq from UCSC genome browser with customized tracks. RNA-seq were collected from siNC ($n = 3$) and si*CLAP* ($n = 3$) injected mice.

C The expression changes of genes upon *CLAP* knockdown by RNA-seq. Differently expressed genes were selected by foldchange ≥ 1.2 and $P \leq 0.05$. Red, blue, green, and gray dots represent upregulated, downregulated, downregulated C2-specific and unchanged genes, respectively.

D The expression changes of C2-specific and itch-related genes upon *CLAP* knockdown by RNA-seq. Each dot represents an RNA-seq sample, and results are presented as mean ± SEM ($n = 3$). $^{*}P < 0.05$, $^{**}P < 0.01$ and $^{***}P < 0.001$ versus siNC.

E Research flowchart for AAV-mediated overexpression of $CLAP^{R}$ by intrathecal injection of AAV-$CLAP^{R}$.

F qPCR showed that downregulated *CLAP* and C2-specific genes including *Sst*, *Plcb3* and *Cysltr2* by si*CLAP* were fully rescued by overexpression of $CLAP^{R}$ in L4/5 DRGs of mice. The results are presented as mean ± SEM (siNC, $n = 10$; si*CLAP*, $n = 6$; si*CLAP* + $CLAP^{R}$, $n = 12$). $^{*}P < 0.01$ versus siNC and $^{\#}P < 0.05$, $^{\#\#}P < 0.01$ versus the indicated treatment.

G qPCR showed the association of *CLAP* with MSI2, but not for *Sst* in mouse DRG following MSI2 RIP experiment. The results are presented as mean ± SEM ($n = 3$). $^{*}P < 0.05$ versus IgG.

H Research flowchart for AAV-mediated overexpression of $CLAP^{R}$ by intrathecal injection of AAV-$CLAP^{R}$.

I qPCR showed that downregulated *Plcb3* by si*CLAP* was fully rescued by knockdown of MSI2 in L4/5 DRGs of mice. The results are presented as mean ± SEM (siNC, $n = 8$; si*CLAP*, $n = 6$; si*CLAP* + siMSI2, $n = 5$). $^{*}P < 0.05$, $^{***}P < 0.001$ versus siNC and $^{\#\#}P < 0.01$ versus the indicated treatment.

Data information: Unpaired *t*-test was used for all statistical analyses.

detecting lower level of lincRNAs in some types of DRG neurons in physiological state. Importantly, many upregulated lincRNAs (Wu *et al*, 2019) and new types of DRG neurons (Wang *et al*, 2021) have been revealed under neuropathic pain, implying more type-specific lincRNAs under pathological conditions such as neuropathic pain and chronic itch.

In the present study, from the composition landscape for neuron-type-specific lincRNAs, > 60% ones were concentrated to only 20% neurons from neuron types C2, C3, and C9, highlighting the possible function of lincRNAs in itch and mechanical sensation. Moreover, we utilized RRA score to rank the neuron-type-specific lincRNAs based on their abundance and specificity as well as consistency in two scRNA-seq methods. RRA ranking provided the priority of unknown lincRNAs for further investigation of their effects in somatosensation. High-ranking candidates such as *CLAP* and *Gm11549* were well validated to localize in specific neuron-type by smFISH and qPCR, and *CLAP* was proven to play a role in neuronal excitation and itch sensation, further suggesting a useful tool of RRA in evaluating the cell-type specificity of genes.

Although most lincRNAs are undetermined for their biological functions in nervous system, the expression and localization of some neuron-type-specific lincRNAs have been reported in previous studies. For instance, *Gm11549* is specifically localized in the 5$^{th}$ layer of mouse cortex (Belgard *et al*, 2011), indicating a potential role with type-specific manner in this layer. Meanwhile, *2310002F09Rik* is specifically enriched in hippocampus but not in the prefrontal cortex (Kadakkuzha *et al*, 2015), implying a tissue-specific expression in central nervous system. More interestingly, *Klk8*, a member of serine protease enzyme family proteins, is gnomically localized nearby *2310002F09Rik* and involved in the progression of psoriasis (Mack & Kim, 2018), strongly implicating a potential role of *2310002F09Rik* in itch sensation. Future studies will be required for its regulatory relationship with kallikrein family protein.

### C2-type-specific lincRNA CLAP contributes to neuron-type specific function

Functional heterogeneity in types and subtypes of somatosensory neurons has been extensively investigated in recent studies (Roberson *et al*, 2013; Chiu *et al*, 2014; Li *et al*, 2016; Stantcheva *et al*, 2016; Solinski *et al*, 2019; Wu *et al*, 2019; Zheng *et al*, 2019; Sharma *et al*, 2020; Pan *et al*, 2021). A population of neurons exclusively expressing *Sst* and *Nppb* have been suggested to be involved in itch and nociceptive transmission (Usoskin *et al*, 2015; Stantcheva *et al*, 2016; Huang *et al*, 2018; Solinski *et al*, 2019). Dysregulated lncRNAs have been reported to be involved in neuropathic pain (Wu *et al*, 2019), especially for upregulated *Kcna2* antisense RNA (Zhao *et al*, 2013) and nerve injury-specific lncRNA (NIS-lncRNA; Du *et al*, 2022) as well as downregulated DRG specifically enriched lncRNA (DS-lncRNA; Pan *et al*, 2021), respectively. However, only a few lncRNAs were identified to be functionally related to physiological somatosensation. Our scRNA-seq identified a conserved lincRNA *CLAP* abundantly localized in the *Sst*-expressing DRG neurons. *CLAP* downregulation or upregulation selectively affected histamine-evoked neuronal activation or scratching in mice, but not other pruritogens such as 5-HT or CQ, suggesting *CLAP* specifically acting in histamine signaling pathway. It should be noted that intrathecal injection of si*CLAP* or AAV-*CLAP* might affect the expression of *CLAP* in spinal cord. *CLAP*-induced itch behavior is possibly not only contributed from the DRG but also the spinal cord.

Several itch-related genes such as *Nppb* and *Il31ra* together with *CLAP* were abundantly and specifically expressed in *Sst*-expressing neurons (Usoskin *et al*, 2015; Li *et al*, 2016, 2018; Solinski *et al*, 2019). RNA-seq of DRGs identified that *CLAP* knockdown *in vivo* reduced the level of several genes specifically expressing in $Sst^{+}$ neurons, which are essential for histamine-mediated scratching (Huang *et al*, 2018; Solinski *et al*, 2019), further suggesting a neuron-type-specific regulation mediated by lincRNA in itch sensation. Furthermore, MSI2 was identified to be an interacting RBP of *CLAP*, and *Plcb3* selected from both MSI2-binding RNAs and *CLAP*-regulated genes was likely regulated by cooperation of *CLAP* and MSI2 because the *CLAP*-regulated *Plcb3* decrease was completely rescued by MSI2 downregulation. These results provide a possibility that *CLAP* regulates itch-related gene via a post-transcriptional role by impeding the MSI2-mediated mRNA decay, which shows a similar way in recent study for lncRNA *ALAE* competing KSHRP on *Gap43* mRNA translation in our laboratory (Wei *et al*, 2021). The precise mechanism for MSI2 and *CLAP* cooperatively in regulating

 

gene expression needs further investigation. Nevertheless, other *CLAP*-regulated gene such as *Sst* did not associate with MSI2, other RBPs in *CLAP*-mediated regulation will be explored.

lincRNAs evolve much faster than protein-coding genes (Ulitsky & Bartel, 2013). Most of conservative lincRNAs have been proven to possess critical functions in different biological processes (Ulitsky & Bartel, 2013; Guo *et al*, 2020). As the most abundant lincRNA among those conserved neuron-type-specific lincRNAs, the function of *CLAP* in mice was not determined. However, the human ortholog of *CLAP*, *LINC00675*, was recently studied and suggested to be a tumor repressor in distinct types of cancer such as gastric, colorectal, and cervical cancers (Ma *et al*, 2018; Shan *et al*, 2018; Zeng *et al*, 2018), implying a potentially regulatory role of this lincRNA in human diseases. More recently, a small protein encoded by *LINC00675* was reported to regulate apoptosis of human colorectal cancer cells (Li *et al*, 2020), indicating that the tumor microenvironment may cause the production of small peptide from *LINC00675*. Despite the conserved region of *CLAP* between human and mouse displays high similarity, sequence variability or distinct secondary structure in non-conserved regions between *CLAP* and *LINC00675* might contribute to undetected coding potential of *CLAP* in mice. Therefore, we speculated that both the sequence variability of *CLAP* with *LINC00675*, and the regulation of cell-type context-dependent translation regulation on lincRNA might affect the translation ability of *CLAP*. Additionally, given the clinical implications of *LINC00675* during tumor progression, *CLAP* might also serve as a potential therapeutic target for itch.

In conclusion, combined two distinct scRNA-seq methods, we provide a resource of neuron-type-specific lincRNAs in somatosensory neurons, which is potentially related to sensory transmission. Our studies will facilitate future exploration for the function of neuron-type-specific lincRNAs in different biological processes.

## Materials and Methods

### Animals

All animal experiments were approved by the Committee of Use of Laboratory in the Shanghai Institute of Biochemistry and Cell Biology, Chinese Academy of Sciences. Mice were raised together with littermates in pathogen-free environment, and their health status was routinely checked. No more than 5 mice were housed in one cage. Mice were maintained in a 12-h light/dark cycle at 22–26°C. Experiments were conducted during the light phase of the cycle. Male mice of 2- to 4-month-old were used for all *in vivo* and *in vitro* experiments.

We generated the mice expressing Ai9 specifically in *Gal*$^+$, *Sst*$^+$, *Slc17a8*$^+$, *Mrgprd*$^+$, or *SNS*$^+$ DRG neurons, respectively, by crossing Ai9-loxP mice with transgenic mice expressing Cre recombinase controlled by promoter of the *Gal*, *Sst*, *Slc17a8*, *Mrgprd* or *SNS* (*Gal-Cre*, *Sst-Cre*, *Slc17a8-Cre*, *Mrgprd-Cre*, *SNS-Cre*). The mice were viable and fertile and did not exhibit visible abnormalities. Ai9-tdTomato mice were purchased from the Jackson Laboratory (Stock No. 007909) and *Mrgprd-Cre* mice were provided by Dr. Jinsong Li's laboratory. C57BL/6J mice were purchased from Shanghai Laboratory Animal Center, Chinese Academy of Sciences (Shanghai, China).

### Cell collection and preliminary data processing for 10× Genomics scRNA-seq

Dissociation of mouse L4/L5 DRGs cells was previously described (Wang *et al*, 2021). Briefly, DRGs were incubated in the DMEM medium containing 1 mg/ml collagenase, 0.4 mg/ml trypsin, and 0.1 mg/ml DNase I for 30 min at 37°C. The myelin debris was removed by 20% Percoll density gradient, and the cells were resuspended in the phosphate buffer saline (PBS) with 0.04% bovine serum albumin (BSA) after dissociation for subsequent 10× Genomics library preparation. Then, the Chromium Next GEM Single Cell 3′ GEM, Library & Gel Bead Kit v2 (PN-120237) was used to construct RNA-seq library. All libraries were sequenced using the Illumina NovaSeq platform.

Mouse genome (mm10) reference with annotation combined from refFlat, knownGene, and ensGene were built using Cell Ranger (version: 3.0.2, parameter: cellranger mkref). Then, 10× Genomics sequencing data were aligned to reference and collapsed unique molecular identifier to obtain gene-cell raw count matrix (parameter: cellranger count). For quality control of each library, R package dropletUtils (Lun *et al*, 2019) was used to remove the ambient background RNA sample and keep the real cells (version: 1.6.1, parameter: FDR $\leq$ 0.01). The cells that the percentage of mitochondrial gene was counted $\geq$ 3% were filtered out. Alignment of different datasets was performed using canonical correlation analysis in Seurat (Stuart *et al*, 2019; version: 3.1.5). And pre-clustering analysis was utilized to distinguish neuronal and non-neuronal cells roughly. Due to their difference of observed gene counts, the neurons and non-neuron cells with < 2,500 and 500 detected genes, respectively, were excluded from subsequent analysis. After above filtering, a total of 7,935 cells were retained for further analysis.

### The data processing for Smart-seq2 scRNA-seq

We performed Smart-seq2 scRNA-seq method as previously reported (Li *et al*, 2016). Briefly, single dissociated L4/L5 DRG neurons were randomly picked and collected into a glass pipette for single-cell RNA extraction. Reverse transcription was using a SMARTer Ultra Low RNA kit (Clontech) and cDNA was amplified by utilizing an Advantage 2 PCR Kit (Clontech) to produce the cDNA library. Finally, cDNA library was sequenced using the Illumine sequencing system (Hiseq 2000).

Smart-seq2 scRNA-seq was aligned to mouse genome with HISAT2 (Kim *et al*, 2019; version: 2.1.0, parameter: --no-softclip --score-min L, -16,0 --mp 7,7 --rfg 0,7 --rdg 0,7 --max-seeds 20), and only uniquely mapped reads were kept for further analysis. Smart-seq2 scRNA-seq data are not using correcting batch effects due to their similar sequencing depth and instrument. Gene counts were calculated for each single cell/sample using featureCounts (Liao *et al*, 2014; version: 1.6.2, parameter: -t exon -g gene_id -O --fraction -p -s 0). Raw gene counts were normalized by transcripts per million (TPM). The TPM of genes was regarded as normalized read count in following analysis.

### Unsupervised clustering and cell-type identification

Cluster analysis of scRNA-seq data was mainly performed with R package Seurat. Gene counts for each cell were normalized by total

counts for that cell and multiplied by one million to create TPM-like values, and the gene counts were computed by natural-log transformed using log (TPM + 1). Variance of each expressed gene was calculated on standardized gene expression value that was generated by a local polynomial regression model in *FindVariableFeatures* function. Top 2000 highly variable genes were used to perform dimension reduction using principal component analysis (PCA). Then, a share neatest neighbor (SNN)-based clustering algorithm was performed on PCA results to identify cell clusters with *FindClusters* function. The 50 principal components with resolution 0.5 were used to perform the first-round cluster and annotated each cluster by known markers for general cell types in dissected DRGs. Nine major cell types were identified in the first-round clustering, including neurons, Schwann cells, satellite cells, immune cells, fibroblasts, VSMCs, VECs, VECCs, and RBCs. The second-round clustering was only performed to get sub-clusters within DRG neurons with resolution 0.6. Finally, 16 types and subtypes of neurons were identified in the second-round clustering, and each cluster was annotated by known markers in the previous study (Li *et al*, 2016). For visualization of cell clusters, the dimensionality of each sample was reduced using t-Distributed Stochastic Neighbor Embedding (t-SNE) with *RunTSNE* function.

#### Gene expression specificity analysis

The expression specificity of genes was evaluated using specificity measure (SPM; Xiao *et al*, 2010) as follows:

$$SPM = \frac{x_i^2}{\sum_{i=1}^{n} x_i^2}$$

Where $\boldsymbol{x}$ is the average expression of genes in each cell type, $\boldsymbol{i}$ is the number of cell types. The value of SPM is between [0, 1], and the expression specificity of a gene is higher as SPM value closer to 1.

#### Aggregating neuron-type-specific lincRNAs in smart-seq2 and 10× Genomics scRNA-seq

To screen significant cell-type-specific lincRNAs, we filtered highly expressed cell-type-specific lincRNAs with $TPM_{mean} \geq 1$ in at least one neuron type and SPM ≥ 0.8. For avoiding technical variance of two methods, we collected lincRNAs by their abundance in each method, and then, we conducted the RRA method to evaluate the significance of each lincRNA using *aggregateRanks* function of R package ROBUSTRANKAGGREG (Kolde *et al*, 2012; version: 1.1, parameter: method = "RRA").

#### Identification of conserved lincRNAs in human and mouse

Conserved lincRNAs were identified with methods described previously (Guo *et al*, 2020). We extracted lincRNAs in human and mouse annotation to conduct sequence and position-conserved analysis. For sequence-conserved lincRNAs, we utilized Blas (Camacho *et al*, 2009) and LiftOver (https://genome.ucsc.edu/cgi-bin/hgLiftOver) tools to evaluate sequence similarity (BLAST: identity ≥ 20%, *E* value ≥ 1 e-5; LiftOver: remapped ratio ≥ 50%, overlapped fraction ≥ 20%) between human and mouse. lincRNA pairs passing both filters were regarded as sequence-conserved lincRNAs. Position-conserved lincRNAs were identified with the conserved promoters and the same position related to nearby conserved protein-coding genes (distance ≤ 50 kb). Conserved promoters were defined as 1,000 bps around transcription start site (TSS) with sequence identity ≥ 10%, and conserved protein-coding genes were downloaded from NCBI HomoloGene database (version build68; https://www.ncbi.nlm.nih.gov/homologene).

#### Weighted gene co-expression network analysis (WGCNA) in neurons

To imply gene regulation in somatosensory neurons, we used R package WGCNA (Langfelder & Horvath, 2008; version: 1.69) to generate gene co-expression network. Briefly, coding genes and lincRNAs with average TPM ≥ 1 and SPM ≥ 0.8 in neuron types were loaded into WGCNA analysis. According to the introductory tutorial, we used the function *pickSoftThreshold* to perform the analysis of network topology and choose a proper soft-thresholding power (powerVector = powers, verbose = 5, networkType = "unsigned"). Then, an unsigned gene co-expression network construction and module detection was performed using *blockwiseModules* function (power = 4, maxBlockSize = 50,000, TOMType = "unsigned", minModuleSize = 30). Top 30 genes of network in each module were visualized using Cytoscape (Otasek *et al*, 2019).

#### Analyzing differential gene expression and gene enrichment

Reads were mapped and counted aforementioned in bulk RNA-seq analysis for each library. The raw counts of genes were loaded to R package DESeq2 (Love *et al*, 2014) and performed the analysis of differential gene expression following guidance. Significant differently expressed genes were filtered with fold change ≥ 1.2 and *P* value ≤ 0.05.

#### Plasmids and antibodies

The full length of *CLAP* was amplified from mouse DRG cDNA and cloned into pCDH.CMV.EF1α.copGFP to produce pCDH.CMV.*CLAP*.EF1α.copGFP and pCDH.CMV.Flag.*CLAP*.EF1α.copGFP. For AAV construction, the shRNA for *CLAP* and scrambled shRNA were cloned into the pAKD.CMV.bGlobin.eGFP.H1.shRNA vector. The AAV2-based vector pseudotyped with AAV9 serotype capsid (AAV2/9) was supplied in titers $5 \times 10^{13}$ (Genetic Reprogramming Platform, Institute of Neuroscience, CAS). The sequences of sh*CLAP* and scrambled shRNA (shNC) were indicated in Appendix Table S1.

Antibodies used in this study were anti-tubulin (Sigma-Aldrich, T5168), anti-GAPDH (Abcam, ab8245), anti-FLAG (Origene, TA50011-100), and anti-MSI2 (Abways, CY5629).

#### Real-time quantitative PCR

For qPCR, total RNA from tissues, cell lysates or beads was extracted using TRIzol reagent (Invitrogen) and subjected to cDNA synthesis using PrimeScript RTase (TaKaRa). qPCR was performed using LightCycler® 96 System (Roche) and Hieff™-qPCR-SYBR®-Green-Master-Mix (Yeasen). The expression of individual gene was

 

calculated by a standard curve and normalized to the expression of *Gapdh*. The PCR primers for genes were shown in Appendix Table S2.

For single-cell PCR, the cDNA library was established as previously reported (Li *et al*, 2016). Briefly, single DRG neuron was manually picked using glass electrode and placed into lysis buffer immediately. The reverse transcription was performed using SuperScript II (Invitrogen), and the product was pre-amplified for 18 cycles using KAPA HiFi HotStart ReadyMix (KAPA Biosystems) to get the cDNA library. Single-cell qPCR was performed as above mentioned. *Gapdh* was used as a positive control, and the clean glass electrode containing extracellular fluid was used as a negative control. The products of qPCR were analyzed on 1% agarose gels.

#### Rapid amplification of cDNA end (RACE)

The method for obtaining the full length of *CLAP* was adopted from previous study (Wang & Fang, 2015). The RNA ligase-mediated (RLM)-RACE approach was performed to obtain the unknown 5′-end and 3′-end sequence of *CLAP* by using SMARTer RACE 5′/3′ kit (Takara) and FirstChoice RLM-RACE Kit (Ambion, Inc.), respectively. Briefly, the 5′RACE and 3′RACE cDNA library was first established from adult DRGs of mice. Then, the RLM-RACE PCR was performed with *CLAP*-specific primers to obtain the product that was further sequenced. Finally, the full-length sequence of *CLAP* was verified by comparing the sequencing result with the RNA-seq data and predicted sequence.

#### Cell culture and transfection

HEK293 cells were obtained from American Type Culture Collection and cultured in DMEM supplemented with 10% fetal bovine serum (GIBCO) and penicillin/streptomycin. Transfection of plasmids in HEK293 cells was performed by lipofectamine 2000 (Invitrogen) according to the manufacturer's protocol.

Primary culture of mouse DRG neurons was previously described (Chen *et al*, 2012) with minor modifications. Briefly, DRGs from 2- to 4-month-old mice were isolated and digested in L15 medium and cultured in the Neurobasal medium containing 2% B27 supplement and 2 mM L-Glutamine (Invitrogen). Dissociated DRG neurons were transfected with the mixture of RNAiMax (Invitrogen) and siRNA in Neurobasal medium. After 6 h, the culture medium was replaced with Neurobasal medium containing 2% B27 supplement and 2 mM L-Glutamine. The neurons were maintained for 48 h for following experiments.

#### Detection of *CLAP* coding potential

The possible ORFs of *CLAP* were predicted using the ORFfinder (https://www.ncbi.nlm.nih.gov/orffinder/) with default parameters. The coding potential of *CLAP* was examined by immunoblotting through inserting a Flag tag into the middle region with three continuous nucleotides, and after the start codon as well as the stop codon of predicted ORF within full-length *CLAP*. The plasmids were transfected into the HEK293 cells with lipofectamine 2000. After 48 h, protein extracts were obtained, separated by sodiumdodecyl sulfate–polyacrylamide gel electrophoresis (SDS–PAGE), transferred, and probed with anti-Flag mouse monoclonal antibody (1:1,000; Origene). Proteins were visualized using enhanced chemiluminescence detection (Amersham Biosciences).

#### smFISH and immunohistochemistry

Wildtype or distinct *Cre*-driven Ai9 mice were perfused with fresh 4% paraformaldehyde (PFA). Then, the DRGs were post-fixed in 4% PFA for 3 h and dehydrated in 20% sucrose overnight at 4°C. Fixed frozen 10-μm sections of DRGs were subjected to the RNAscope-based signal amplification (Advanced Cell Diagnostics) followed by immunohistochemistry. Briefly, the slices were first treated with hydrogen peroxide for 10 min at room temperature and applied with boiling retrieval solution for 5 min. Next, Protease III was used to penetrate the membrane for 10 min at 40°C. For hybridization, slides were incubated with *C530044C16Rik*, *9130409J20Rik* (*CLAP*), *Gm11549* and *2310002F09Rik* probe, respectively, for 2 h at 40°C. For signal amplifying, slices were incubated with amplification solution, followed by TSA Plus Fluorescein. After *in situ* hybridization, slides were incubated with the indicated primary antibody overnight at 4°C, followed by secondary antibodies for 30 min at 37°C. Images were acquired on a spinning disk confocal microscope (ANDOR) and SP8 confocal microscope (Leica).

Quantitative analysis for the percentage of lincRNAs in distinct types of DRG neurons was performed by CellSens Dimension software (Olympus). Briefly, $NeuN^+$ cells in DRG sections were collected, and the positive spots with the mean area larger than 5 $pixel^2$ were analyzed by the software. Meanwhile, the threshold of spot numbers for each slice was set based on the average spots of lincRNA showing in all $tdTomato^+$ neurons. Neurons exceeding the threshold spots were counted as lincRNA highly expressed. Finally, the percentage of colocalization was calculated by the number of neurons highly expressed lincRNA versus total number of $tdTomato^+$ neurons. At least 6 DRGs from 3 mice per group were analyzed. For the quantification of subcellular localization for the neuron-type-specific lincRNAs, the number of spots in cytoplasm and nucleus from at least 20 neurons of 3 mice was analyzed. Finally, the percentage of lincRNAs in cytoplasm and nucleus was calculated.

#### Intrathecal injection of siRNA and AAV

Intrathecal injection of siRNA was performed as described previously (Wang *et al*, 2021). Briefly, the mice were intrathecally injected with 2 times of 6 μg siNC or si*CLAP* which were modified with 2′-O-methyl and 5′-cholesterol in every other day, and then performed behavioral tests after 24 h. For AAV treatment, the mice were intrathecally injected with $1 \times 10^{11}$ vg of AAV-shNC and AAV-sh*CLAP* as well as AAV-*CLAP* and -$CLAP^R$ (without siRNA target sequence) once, and performed behavioral tests after 30 days. Then, the L4/5 DRGs were harvested for RNA extraction and qPCR analysis for the detection of the knockdown efficiency of siRNA and shRNA.

#### FACS

DRG cells from *Sst-Cre*; Ai9 and *SNS-Cre*; Ai9 mice were collected, washed, resuspended in ice-cold PBS and filtered through a strainer. FACS of tdTomato-positive neurons was performed by SONY

MA900 multi-application cell sorter (SONY) after eliminating the dead cells. The sorted tdTomato$^+$ DRG neurons were plated on glass-bottom dish pre-coated with poly-D-lysine. After 48-h culture, these DRG neurons were used for RNA extraction and qPCR analysis for the detection of neuron-type-specific lincRNAs and mRNAs.

#### Calcium imaging

The dissociated DRG neurons from 4 *Sst-Cre*; Ai9 mice were plated on the glass coverslip and incubated with 10 μM Fura-2-AM (Molecular Probes) in HBSS solution for 30 min. Then, the glass coverslip was placed into a chamber and perfused with extracellular solution (NaCl 140 mM, KCl 5 mM, HEPES 10 mM, $CaCl_2$ 2 mM, $MgCl_2$ 2 mM, glucose 10 mM). DRG neurons were imaged at 340-nm and 380-nm excitation to detect intracellular free $Ca^{2+}$ by Nikon A1R confocal microscopy (Nikon). The $Ca^{2+}$ influx curve represented a normalized value of the ratio for fluorescent difference (Ft − F0) to basal fluorescence (F0). Cells were identified as responsive neuron based on the calcium elevation measured by the average ratio (340 nm/380 nm) after 10 s treatment by different drugs was 15% above baseline as previous study (Dong *et al*, 2020). Histamine (1 mM, Sigma), 5-HT (100 μM, Tocris Bioscience), chloroquine (1 mM, Sigma), capsaicin (1 μM, Sigma), and KCl (80 mM, Sigma) were applied to DRG neurons to observe $Ca^{2+}$ influx. The percentage of drug-responsive tdTomato$^+$ neurons was calculated in the pool of KCl-responsive cells. At least 300 KCl-responsive tdTomato$^+$ neurons were analyzed from 4 independent experiments. NIS-Elements (version 3.1, Nikon) and Prism 6 (version 6.0 e, GraphPad) were used to analyze $Ca^{2+}$ imaging data.

#### Behavioral tests for itch, mechanical, thermal, and cold response

Behavioral tests were performed with 2- to 4-month-old male mice. In the hot plate, cold plate, and von Frey tests, the response latency to nociceptive stimuli was recorded. Above tests were stopped at a cutoff time or force for animal protection.

Acute itch test was performed according to previous report (Han *et al*, 2018). After intrathecal injection of siRNA or AAV-shRNA, mice were shaved on the nape. Mice were intradermally injected with distinct pruritogens including histamine (500 μg), 5-HT (10 μg) and chloroquine (200 μg), respectively, into the nape of the neck (50 μl). The number of hindlimb scratching bouts was recorded by high-resolution camera and counted for 30 min. A bout of scratching was defined as a lifting of the hindlimb toward the injection site and then a replacing of the limb back to the floor. Scratching behavior was qualified by counting the number of scratching bouts over the 30-min observation period.

Mechanical pain test was performed based on previous report (Yang *et al*, 2017). Briefly, the von Frey filaments with forces of increasing grades were applied to the hind paw of mice. One filament was applied 5 times in a round of testing. The filament force inducing paw withdrawal for more than 3 times in a round of testing was defined as the mechanical threshold.

For the test of thermal sensitivity, mice were put on a hot (52°C) or cold (4°C) plate. The withdrawal latency was the time when tested mice showed a sign of lifting and licking hind paws or jumping, and represented the degree of nociceptive threshold. The cutoff time is 30 s.

#### RNA immunoprecipitation (RIP)

RIP experiments were performed as previous report (Wei *et al*, 2021). Briefly, adult mice DRG tissues were harvested and lysed with RIPA buffer (100 mM KCl, 5 mM $MgCl_2$, 10 mM HEPES-NaOH, 0.5% NP-40) with RNase inhibitor (Promega) and protease inhibitor cocktail (Roche). Then, 1 μg MSI2 antibody was incubated with 50 μl protein G beads (Sigma) at room temperature for 1 h in the washing buffer (50 mM Tris, pH 7.4; 150 mM NaCl, 1 mM $MgCl_2$, 0.05% NP-40). Then, the resulting supernatant was incubated with the antibody conjugated with immobilized beads at 4°C for 3 h. The same amount of IgG was used as a control. RNA extraction and immunoblotting from the beads were further carried out by using TRIzol (Invitrogen) and loading buffer, respectively, for subsequent detection of co-immunoprecipitated RNA and protein.

#### Statistical analysis

All data are presented as the mean ± SEM. Statistical analyses for all experiments were performed using two-tailed paired Student's *t*-tests in Prism (GraphPad Software). Differences were considered significant at $P < 0.05$.

## Data availability

In our previous research, the datasets of Smart-seq2 and 10× Genomics were deposited to Gene Expression Omnibus with the accessed number GSE63576 (https://www.ncbi.nlm.nih.gov/geo/query/acc.cgi?acc=GSE63576) and GSE155622 (https://www.ncbi.nlm.nih.gov/geo/query/acc.cgi?acc=GSE155622), respectively. The datasets of RNA-seq from siNC and si*CLAP* of DRGs are available in the GSE168832 (https://www.ncbi.nlm.nih.gov/geo/query/acc.cgi?acc=GSE168832).

**Expanded View** for this article is available online.

### Acknowledgements
We thank Dr. Zhenzhong Xu (Zhejiang University School of Medicine) for the help of detecting *CLAP* in human DRG and the Core Facility of Shanghai Research Center for Brain Science and Brain-Inspired Intelligence for providing technical support. This work was supported by grants from National Natural Science Foundation of China (32070968 and 32070967), Guangdong High Level Innovation Research Institute (2021B0909050004) and Innovation Fund for Medical Sciences of Chinese Academy of Medical Sciences (2019-12M-5-082).

### Author contributions
**Bin Wang:** Conceptualization; data curation; formal analysis; funding acquisition; investigation; writing—original draft; project administration; writing—review and editing. **Bowen Jiang:** Data curation; software; investigation; methodology; writing—original draft. **Guo-Wei Li:** Resources; data curation; software; writing—original draft. **Fei Dong:** Investigation. **Zheng Luo:** Software; methodology. **Bing Cai:** Investigation. **Manyi Wei:** Investigation. **Jiansong Huang:** Investigation. **Kaikai Wang:** Data curation. **Xin Feng:** Investigation. **Fang Tong:** Investigation. **Sashuang Wang:** Investigation. **Qiong Wang:** Data curation. **Qingjian Han:** Data curation. **Changlin Li:** Data curation; methodology. **Xu Zhang:** Conceptualization. **Li**

 

**Yang:** Conceptualization; supervision; writing—review and editing. **Lan Bao:** Conceptualization; formal analysis; supervision; funding acquisition; writing—original draft; project administration; writing—review and editing.

### Disclosure and competing interests statement

The authors declare that they have no conflict of interest.

## References


Basbaum AI, Bautista DM, Scherrer G, Julius D (2009) Cellular and molecular mechanisms of pain. *Cell* 139: 267–284

Belgard TG, Marques AC, Oliver PL, Abaan HO, Sirey TM, Hoerder-Suabedissen A, Garcia-Moreno F, Molnar Z, Margulies EH, Ponting CP (2011) A transcriptomic atlas of mouse neocortical layers. *Neuron* 71: 605–616

Bennett CG, Riemondy K, Chapnick DA, Bunker E, Liu X, Kuersten S, Yi R (2016) Genome-wide analysis of Musashi-2 targets reveals novel functions in governing epithelial cell migration. *Nucleic Acids Res* 44: 3788–3800

Briggs JA, Wolvetang EJ, Mattick JS, Rinn JL, Barry G (2015) Mechanisms of long non-coding RNAs in mammalian nervous system development, plasticity, disease, and evolution. *Neuron* 88: 861–877

Cabili MN, Trapnell C, Goff L, Koziol M, Tazon-Vega B, Regev A, Rinn JL (2011) Integrative annotation of human large intergenic noncoding RNAs reveals global properties and specific subclasses. *Genes Dev* 25: 1915–1927

Camacho C, Coulouris G, Avagyan V, Ma N, Papadopoulos J, Bealer K, Madden TL (2009) BLAST+: architecture and applications. *BMC Bioinformatics* 10: 421

Carlevaro-Fita J, Johnson R (2019) Global positioning system: understanding long noncoding RNAs through subcellular localization. *Mol Cell* 73: 869–883

Chen LL (2016) Linking long noncoding RNA localization and function. *Trends Biochem Sci* 41: 761–772

Chen XQ, Wang B, Wu C, Pan J, Yuan B, Su YY, Jiang XY, Zhang X, Bao L (2012) Endosome-mediated retrograde axonal transport of P2X3 receptor signals in primary sensory neurons. *Cell Res* 22: 677–696

Chiu IM, Barrett LB, Williams EK, Strochlic DE, Lee S, Weyer AD, Lou S, Bryman GS, Roberson DP, Ghasemlou N *et al* (2014) Transcriptional profiling at whole population and single cell levels reveals somatosensory neuron molecular diversity. *eLife* 3: e04660

Dong X, Dong X (2018) Peripheral and central mechanisms of itch. *Neuron* 98: 482–494

Dong F, Shi H, Yang L, Xue H, Wei M, Zhong YQ, Bao L, Zhang X (2020) FGF13 is required for histamine-induced itch sensation by interaction with $Na_V1.7$. *J Neurosci* 40: 9589–9601

Du S, Wu S, Feng X, Wang B, Xia S, Liang L, Zhang L, Govindarajalu G, Bunk A, Kadakia F *et al* (2022) A nerve injury-specific long noncoding RNA promotes neuropathic pain by increasing Ccl2 expression. *J Clin Invest* 132: e153563

Guo CJ, Ma XK, Xing YH, Zheng CC, Xu YF, Shan L, Zhang J, Wang S, Wang Y, Carmichael GG *et al* (2020) Distinct processing of lncRNAs contributes to non-conserved functions in stem cells. *Cell* 181: 621–636

Han SK, Mancino V, Simon MI (2006) Phospholipase Cbeta 3 mediates the scratching response activated by the histamine H1 receptor on C-fiber nociceptive neurons. *Neuron* 52: 691–703

Han L, Ma C, Liu Q, Weng HJ, Cui Y, Tang Z, Kim Y, Nie H, Qu L, Patel KN *et al* (2013) A subpopulation of nociceptors specifically linked to itch. *Nat Neurosci* 16: 174–182

Han Q, Liu D, Convertino M, Wang Z, Jiang C, Kim YH, Luo X, Zhang X, Nackley A, Dokholyan NV *et al* (2018) miRNA-711 binds and activates TRPA1 extracellularly to evoke acute and chronic pruritus. *Neuron* 99: 449–463

Huang J, Polgar E, Solinski HJ, Mishra SK, Tseng PY, Iwagaki N, Boyle KA, Dickie AC, Kriegbaum MC, Wildner H *et al* (2018) Circuit dissection of the role of somatostatin in itch and pain. *Nat Neurosci* 21: 707–716

Kadakkuzha BM, Liu XA, McCrate J, Shankar G, Rizzo V, Afinogenova A, Young B, Fallahi M, Carvalloza AC, Raveendra B *et al* (2015) Transcriptome analyses of adult mouse brain reveal enrichment of lncRNAs in specific brain regions and neuronal populations. *Front Cell Neurosci* 9: 63

Kim D, Paggi JM, Park C, Bennett C, Salzberg SL (2019) Graph-based genome alignment and genotyping with HISAT2 and HISAT-genotype. *Nat Biotechnol* 37: 907–915

Kolde R, Laur S, Adler P, Vilo J (2012) Robust rank aggregation for gene list integration and meta-analysis. *Bioinformatics* 28: 573–580

Langfelder P, Horvath S (2008) WGCNA: an R package for weighted correlation network analysis. *BMC Bioinformatics* 9: 559

Li CL, Li KC, Wu D, Chen Y, Luo H, Zhao JR, Wang SS, Sun MM, Lu YJ, Zhong YQ *et al* (2016) Somatosensory neuron types identified by high-coverage single-cell RNA-sequencing and functional heterogeneity. *Cell Res* 26: 83–102

Li C, Wang S, Chen Y, Zhang X (2018) Somatosensory neuron typing with high-coverage single-cell RNA sequencing and functional analysis. *Neurosci Bull* 34: 200–207

Li XL, Pongor L, Tang W, Das S, Muys BR, Jones MF, Lazar SB, Dangelmaier EA, Hartford CC, Grammatikakis I *et al* (2020) A small protein encoded by a putative lncRNA regulates apoptosis and tumorigenicity in human colorectal cancer cells. *eLife* 9: e53734

Liao Y, Smyth GK, Shi W (2014) featureCounts: an efficient general purpose program for assigning sequence reads to genomic features. *Bioinformatics* 30: 923–930

Liu SJ, Nowakowski TJ, Pollen AA, Lui JH, Horlbeck MA, Attenello FJ, He D, Weissman JS, Kriegstein AR, Diaz AA *et al* (2016) Single-cell analysis of long non-coding RNAs in the developing human neocortex. *Genome Biol* 17: 67

Love MI, Huber W, Anders S (2014) Moderated estimation of fold change and dispersion for RNA-seq data with DESeq2. *Genome Biol* 15: 550

Lun ATL, Riesenfeld S, Andrews T, Dao TP, Gomes T, participants in the 1st Human, Cell Atlas J, Marioni JC (2019) EmptyDrops: distinguishing cells from empty droplets in droplet-based single-cell RNA sequencing data. *Genome Biol* 20: 63

Ma S, Deng X, Yang Y, Zhang Q, Zhou T, Liu Z (2018) The lncRNA LINC00675 regulates cell proliferation, migration, and invasion by affecting Wnt/beta-catenin signaling in cervical cancer. *Biomed Pharmacother* 108: 1686–1693

Mack MR, Kim BS (2018) The itch-scratch cycle: a neuroimmune perspective. *Trends Immunol* 39: 980–991

Madisen L, Zwingman TA, Sunkin SM, Oh SW, Zariwala HA, Gu H, Ng LL, Palmiter RD, Hawrylycz MJ, Jones AR *et al* (2010) A robust and high-throughput Cre reporting and characterization system for the whole mouse brain. *Nat Neurosci* 13: 133–140

Mantsoki A, Devailly G, Joshi A (2016) Gene expression variability in mammalian embryonic stem cells using single cell RNA-seq data. *Comput Biol Chem* 63: 52–61

Olsen TK, Baryawno N (2018) Introduction to single-cell RNA sequencing. *Curr Protoc Mol Biol* 122: e57

Otasek D, Morris JH, Boucas J, Pico AR, Demchak B (2019) Cytoscape automation: empowering workflow-based network analysis. *Genome Biol* 20: 185

Pan Z, Du S, Wang K, Guo X, Mao Q, Feng X, Huang L, Wu S, Hou B, Chang YJ *et al* (2021) Downregulation of a dorsal root ganglion-

specifically enriched long noncoding RNA is required for neuropathic pain by negatively regulating RALY-triggered Ehmt2 expression. *Adv Sci* 8: e2004515

Perry RB, Hezroni H, Goldrich MJ, Ulitsky I (2018) Regulation of neuroregeneration by long noncoding RNAs. *Mol Cell* 72: 553–567

Ransohoff JD, Wei Y, Khavari PA (2018) The functions and unique features of long intergenic non-coding RNA. *Nat Rev Mol Cell Biol* 19: 143–157

Roberson DP, Gudes S, Sprague JM, Patoski HA, Robson VK, Blasl F, Duan B, Oh SB, Bean BP, Ma Q *et al* (2013) Activity-dependent silencing reveals functionally distinct itch-generating sensory neurons. *Nat Neurosci* 16: 910–918

Salta E, De Strooper B (2017) Noncoding RNAs in neurodegeneration. *Nat Rev Neurosci* 18: 627–640

Shan Z, An N, Qin J, Yang J, Sun H, Yang W (2018) Long non-coding RNA Linc00675 suppresses cell proliferation and metastasis in colorectal cancer via acting on miR-942 and Wnt/beta-catenin signaling. *Biomed Pharmacother* 101: 769–776

Sharma N, Flaherty K, Lezgiyeva K, Wagner DE, Klein AM, Ginty DD (2020) The emergence of transcriptional identity in somatosensory neurons. *Nature* 577: 392–398

Solinski HJ, Kriegbaum MC, Tseng PY, Earnest TW, Gu X, Barik A, Chesler AT, Hoon MA (2019) Nppb neurons are sensors of mast cell-induced itch. *Cell Rep* 26: 3561–3573

Stantcheva KK, Iovino L, Dhandapani R, Martinez C, Castaldi L, Nocchi L, Perlas E, Portulano C, Pesaresi M, Shirlekar KS *et al* (2016) A subpopulation of itch-sensing neurons marked by ret and somatostatin expression. *EMBO Rep* 17: 585–600

Stuart T, Butler A, Hoffman P, Hafemeister C, Papalexi E, Mauck WM 3rd, Hao Y, Stoeckius M, Smibert P, Satija R (2019) Comprehensive integration of single-cell data. *Cell* 177: 1888–1902

Ulitsky I (2016) Evolution to the rescue: using comparative genomics to understand long non-coding RNAs. *Nat Rev Genet* 17: 601–614

Ulitsky I, Bartel DP (2013) lincRNAs: genomics, evolution, and mechanisms. *Cell* 154: 26–46

Usoskin D, Furlan A, Islam S, Abdo H, Lonnerberg P, Lou D, Hjerling-Leffler J, Haeggstrom J, Kharchenko O, Kharchenko PV *et al* (2015) Unbiased classification of sensory neuron types by large-scale single-cell RNA sequencing. *Nat Neurosci* 18: 145–153

Wang C, Fang J (2015) RLM-RACE, PPM-RACE, and qRT-PCR: an integrated strategy to accurately validate miRNA target genes. *Methods Mol Biol* 1296: 175–186

Wang K, Wang S, Chen Y, Wu D, Hu X, Lu Y, Wang L, Bao L, Li C, Zhang X (2021) Single-cell transcriptomic analysis of somatosensory neurons uncovers temporal development of neuropathic pain. *Cell Res* 31: 904–918

Wei M, Huang J, Li GW, Jiang B, Cheng H, Liu X, Jiang X, Zhang X, Yang L, Bao L *et al* (2021) Axon-enriched lincRNA ALAE is required for axon elongation via regulation of local mRNA translation. *Cell Rep* 35: 109053

Wu S, Bono J, Tao YX (2019) Long noncoding RNA (lncRNA): a target in neuropathic pain. *Expert Opin Ther Targets* 23: 15–20

Xiao SJ, Zhang C, Zou Q, Ji ZL (2010) TiSGeD: a database for tissue-specific genes. *Bioinformatics* 26: 1273–1275

Yang L, Dong F, Yang Q, Yang PF, Wu R, Wu QF, Wu D, Li CL, Zhong YQ, Lu YJ *et al* (2017) FGF13 selectively regulates heat nociception by interacting with Nav1.7. *Neuron* 93: 806–821

Yao RW, Wang Y, Chen LL (2019) Cellular functions of long noncoding RNAs. *Nat Cell Biol* 21: 542–551

Zeisel A, Hochgerner H, Lonnerberg P, Johnsson A, Memic F, van der Zwan J, Haring M, Braun E, Borm LE, La Manno G *et al* (2018) Molecular architecture of the mouse nervous system. *Cell* 174: 999–1014

Zeng S, Xie X, Xiao YF, Tang B, Hu CJ, Wang SM, Wu YY, Dong H, Li BS, Yang SM (2018) Long noncoding RNA LINC00675 enhances phosphorylation of vimentin on Ser83 to suppress gastric cancer progression. *Cancer Lett* 412: 179–187

Zhang Q, He Y, Luo N, Patel SJ, Han Y, Gao R, Modak M, Carotta S, Haslinger C, Kind D *et al* (2019) Landscape and dynamics of single immune cells in hepatocellular carcinoma. *Cell* 179: 829–845

Zhao X, Tang Z, Zhang H, Atianjoh FE, Zhao JY, Liang L, Wang W, Guan X, Kao SC, Tiwari V *et al* (2013) A long noncoding RNA contributes to neuropathic pain by silencing Kcna2 in primary afferent neurons. *Nat Neurosci* 16: 1024–1031

Zheng Y, Liu P, Bai L, Trimmer JS, Bean BP, Ginty DD (2019) Deep sequencing of somatosensory neurons reveals molecular determinants of intrinsic physiological properties. *Neuron* 103: 598–616

Ziegenhain C, Vieth B, Parekh S, Reinius B, Guillaumet-Adkins A, Smets M, Leonhardt H, Heyn H, Hellmann I, Enard W (2017) Comparative analysis of single-cell RNA sequencing methods. *Mol Cell* 65: 631–643

Zou M, Li S, Klein WH, Xiang M (2012) Brn3a/Pou4f1 regulates dorsal root ganglion sensory neuron specification and axonal projection into the spinal cord. *Dev Biol* 364: 114–127

Zou H, Luo J, Guo Y, Liu Y, Wang Y, Deng L, Li P (2022) RNA-binding protein complex LIN28/MSI2 enhances cancer stem cell-like properties by modulating hippo-YAP1 signaling and independently of Let-7. *Oncogene* 41: 1657–1672

 